MARTIN MARIETTA ENERGY SYSTEMS LIBRARIES
3 4456 0361397 1

CRL
4
CENTRAL RESEARCH LIBRARY
DOCUMENT COLLECTION

ORNL-2775
Physics and Mathematics

MEASUREMENT OF STOPPING POWER OF COPPER BY CALORIMETRIC METHODS

P. L. Ziemer
R. M. Johnson
R. D. Birkhoff

CENTRAL RESEARCH LIBRARY
DOCUMENT COLLECTION
LIBRARY LOAN COPY
DO NOT TRANSFER TO ANOTHER PERSON
If you wish someone else to see this document, send in name with document and the library will arrange a loan.

OAK RIDGE NATIONAL LABORATORY
operated by
UNION CARBIDE CORPORATION
for the
U.S. ATOMIC ENERGY COMMISSION

Printed in USA. Price $2.75. Available from the

Office of Technical Services
Department of Commerce
Washington 25, D.C.

LEGAL NOTICE

This report was prepared as an account of Government sponsored work. Neither the United States, nor the Commission, nor any person acting on behalf of the Commission:

A. Makes any warranty or representation, expressed or implied, with respect to the accuracy, completeness, or usefulness of the information contained in this report, or that the use of any information, apparatus, method, or process disclosed in this report may not infringe privately owned rights; or

B. Assumes any liabilities with respect to the use of, or for damages resulting from the use of any information, apparatus, method, or process disclosed in this report.

As used in the above, "person acting on behalf of the Commission" includes any employee or contractor of the Commission, or employee of such contractor, to the extent that such employee or contractor of the Commission, or employee of such contractor prepares, disseminates, or provides access to, any information pursuant to his employment or contract with the Commission, or his employment with such contractor.

ORNL-2775

Contract No. W-7405-eng-26

HEALTH PHYSICS DIVISION

MEASUREMENT OF STOPPING POWER OF COPPER BY CALORIMETRIC METHODS

P. L. Ziemer
R. M. Johnson
R. D. Birkhoff

Submitted as a thesis to the Faculty of the Graduate School of Vanderbilt University in partial fulfillment of the requirements for the degree of Master of Science in physics.

DATE ISSUED

DEC 17 1959

OAK RIDGE NATIONAL LABORATORY
Oak Ridge, Tennessee
operated by
UNION CARBIDE CORPORATION
for the
U. S. ATOMIC ENERGY COMMISSION

MARTIN MARIETTA ENERGY SYSTEMS LIBRARIES

3 4456 0361397 1

ACKNOWLEDGMENTS

The author takes pleasure in expressing his sincere appreciation to Dr. R. D. Birkhoff of the Health Physics Division, Oak Ridge National Laboratory, who initiated and directed this work.

Appreciation is extended to Dr. H. H. Hubbell, Jr., for his helpful comments and assistance in all phases of the investigation; to R. M. Johnson who was responsible for the design of the electron gun and the vacuum evaporator; and to H. F. Holzer for his assistance with the electronics.

This investigation was performed at the Oak Ridge National Laboratory under the provisions of an Atomic Energy Commission Fellowship in Radiological Physics. Grateful acknowledgment is made to W. W. Grigorieff of the Oak Ridge Institute of Nuclear Studies who administered the fellowship. Further appreciation is extended to Dr. E. E. Anderson of the Health Physics Division, Oak Ridge National Laboratory, for her interest and advice.

TABLE OF CONTENTS

	Page
Acknowledgments	ii
List of Tables	vi
List of Figures	vii
I. Introduction and Summary of Previous Calorimetric Radiation Measurements	1
II. Theory	12
A. Stopping Power	12
B. Calorimetry	13
1. The Fundamental Heat Equation	13
2. The Drift Method	15
a. Equation for the Power Loss in the Foil	15
b. Theoretical Determination of Heat Loss Constant K_2	17
c. Theoretical Determination of Calibration Constant K_1	19
3. The Null Method	22
4. Relation Between Drift Method and Null Method	26
C. Nuclear Scattering Effects	27
1. Single Scattering and Extraneous Heating	27
2. Multiple Scattering and Increased Path Length	36
III. Apparatus	38
A. Gun and Power Supply	38
1. Electron Gun	38
2. Power Supply	43

TABLE OF CONTENTS CON'T

		Page
III.	Apparatus (Con't)	
	B. Accelerator	45
	C. Apparatus for Measuring Energy Loss	48
	1. Temperature Control	48
	2. Apparatus for Measuring Temperature Rise in the Foil	50
	3. Apparatus for Measuring Beam Current	54
	4. Auxiliary Equipment	56
IV.	Techniques for Making Foils	59
	A. The Vacuum Evaporator	59
	1. Pumping System	59
	2. Evaporation Chamber and Electrical Services	61
	B. Techniques of Foil Preparation	61
	1. Preparation of Glass Slides	61
	2. Filaments	65
	3. Evaporation Procedures	70
	4. Removal of Foil from Glass Slide and Mounting of Foil	71
	C. Weighing the Foils	72
	1. The Modified Electrobalance	72
	2. Calibration of Electrobalance	73
V.	Procedure and Results	79
	A. Determination of $\overline{\Delta E}_{app}$	79
	B. Determination of $\overline{\Delta x}$	84
	C. Apparent Stopping Power	85
	D. Results	85

TABLE OF CONTENTS CON'T

		Page
VI.	Conclusions	87
	Appendices	
I.	Temperature Distribution in Thermocouple Wires	88
II.	Temperature Gradient in Foil	92
III.	Data	94
IV.	Sample Calculation	96
V.	Error Analysis	104
	Bibliography	107

LIST OF TABLES

		Page
I.	Backing Materials	66
II.	Filament and Foil Vapor Sources	69
III.	Calibration Data for Electrobalance	77
IV.	Data for 191.8 $\mu g/cm^2$ Copper	95
V.	Calibration Run for Copper	97
VI.	Data for 51.56 Kev Electrons	100
VII.	Path Length Corrections for 191.8 $\mu g/cm^2$ Copper	103

LIST OF FIGURES

		Page
1.	Equivalent Circuit for Temperature Monitoring Thermopile	21
2.	Use of Peltier Effect for Cooling Foil	24
3.	Spencer's Ratio for $\theta = 101^\circ$	30
4.	Single Scattering of Primary Electrons into Foil Mounting Ring	31
5.	Apparent Energy Loss as a Function of the Scattered Fraction of the Beam	34
6.	Bias Disc Current Due to Scattering at Various Energies	35
7.	Schematic Diagram of the Apparatus	39
8.	Cross Section of Electron Gun and Mount	40
9.	The Electron Gun and Filament	41
10.	Electron Gun Power Supply	44
11.	Schematic Diagram of Apparatus for Measuring Beam Current and Foil Temperature	46
12.	Dissassembled View of Apparatus for Measuring Beam Current and Foil Temperature	49
13.	Heat Sink and Foil Mount With Foil in Place in Center	51
14.	Cutaway of Heat Sink and Foil Mount Showing Wiring for One Thermopile	53
15.	Bias Disc Current as a Function of Bias Voltage	57
16.	The Vacuum Evaporation Chamber Showing Glass Slides on Support Stand and Electrodes	62
17.	Technique for Removal of Foil from Glass Slide	64
18.	Modified Circuit for Cahn Electrobalance	74

LIST OF FIGURES CON'T

		Page
19.	Cahn Electrobalance with Modifications	75
20.	Calibration of Cahn Electrobalance	78
21.	Determination of K_{2t}	81
22.	Stopping Power for 191.8 $\mu g/cm^2$ Copper	86
23.	Temperature Distribution in a Current Carrying Conductor	91

ABSTRACT

The electron stopping power of copper was determined by measuring directly the power dissipated as heat in a copper foil by a transmitted beam of monoenergetic electrons. Monoenergetic electrons from an electron gun were accelerated by a linear accelerator and impinged normally on a 191.8 microgram per square centimeter copper foil. The electron beam was varied from $31._{56}$ to $126._{56}$ Kev in steps of 10 Kev, and the heating effect was determined at each energy. The power dissipated as heat was measured using a set of six copper-constantan thermocouples. The ratio of this power loss to the current of the electrom beam passing through the foil gave the average energy loss, $\overline{\Delta E}$, for each incident energy. The thermocouple system was calibrated by lowering the beam energy below 2.5 Kev so that the beam was completely absorbed in the foil. Foils were prepared by vacuum evaporation onto a water soluble coating on a glass slide. Details of technique of evaporation and mounting are given. The path length for the bombarding electrons corresponded to the foil thickness, $\overline{\Delta x}$, and was determined by weighing a known area (0.987 cm^2) of foil. Corrections were made for single and multiple scattering effects, and the stopping power was then given by the ratio $\frac{\overline{\Delta E}}{\overline{\Delta x}}$. The probable error was calculated and found to be 3.7%. For all energies examined agreement was found with Bethe's expression for electron stopping power.

I. INTRODUCTION AND SUMMARY OF PREVIOUS CALORIMETRIC RADIATION MEASUREMENTS

If a beam of charged particles of kinetic energy E_1 impinges normally on an absorbing medium of thickness Δx, the beam will emerge with some average energy $\overline{E_2}$. One then defines the stopping power of the medium as the average rate of energy loss for the particle. That is, the stopping power of the medium is defined with respect to the kind and energy of the bombarding particles. This may be written in a general way as

$$-\frac{dE}{dx} \equiv \lim_{\Delta x \to 0} \frac{\overline{E_2} - E_1}{\Delta x} \tag{1}$$

where $-\frac{dE}{dx}$ is negative indicating an energy loss.

In the case of stopping power for electrons, the energy losses occur primarily by collisions of the bombarding electrons with the orbital electrons of the absorber. In addition, the incident electrons may be scattered by the nuclei of the absorber without energy transfer. This scattering results in an increase in the effective path length over the stopping foil for the incident electrons. These two effects are largely responsible for the absorption of an electron beam as it penetrates a medium.

A basic reason for making stopping power measurements is to present a general picture of the energy transfer that occurs when a charged particle passes through an absorbing medium. Interest in stopping power

arises not only because it is a basic physical phenomenon but because it is important in the field of Health Physics. Dosimetry measurements depend upon a knowledge of stopping power as it is used in the well-known Bragg-Gray principle. Also, stopping power plays an important role in studying chemical and biological radiation effects.

The phenomenon of stopping power was first discovered experimentally by Leithäuser[1] in 1904, and treated theoretically by Bohr[2] in 1913. The theory was developed within the framework of quantum mechanics by Bethe[3] in 1930. Then in 1933, Bloch[4] applied the statistical model to Bethe's theory giving the stopping power as a simple function of the atomic number of the stopping atom. In 1939 Fermi[5] considered the effect of the polarization of the medium on the stopping power. Thus the theory of stopping power was well developed by the early 1940's.

Although stopping power theory is well developed, little quantitative experimental work with electrons has been reported in the literature. In the most recent review of the subject, Birkhoff[6] has discussed in some detail the work done by a number of early experimenters such as Leithäuser, Whiddington, Terrill, Becker, and Madgwick. Little can be concluded about

---

[1] G. Leithäuser, Ann. Phys. 15, 283 (1904).
[2] N. Bohr, Phil. Mag., 25, 10 (1913).
[3] H. Bethe, Ann. Phys., 5, 325 (1930).
[4] F. Bloch, Z. Phys., 81, 363 (1933).
[5] E. Fermi, Phys. Rev., 56, 1242 (1939).
[6] R. D. Birkhoff, Handbuch der Physik, 34, 53 (1958).

stopping power from these early works because of the problems which were encountered involving scattering, resolving power, and distortion of the straggling distributions which were observed.

The significant point in the measurement of stopping power as described herein is that the energy imparted to the medium under consideration was measured directly by calorimetric methods. This technique, which was a continuation of the work initiated by Kalil, Stone, Hubbell and Birkhoff[7], provided a method of measuring stopping power that was consistent with the definition of electron stopping power. That is, by measuring the energy dissipated as heat, one measured directly the average rate of energy loss of all electrons which passed through the absorbing medium. It was assumed that all energy losses were dissipated as heat. There could be no appreciable stored energy due to chemical changes because only elemental metals were used. Further, no lattice changes were possible for the energies used. For example, in the case of a 130Kev electron striking a copper atom, the maximum energy imparted to the atom is of the order of 5 eV. This is well below the energy necessary for a lattice change which Seitz and Koehler[8] state to be about 25 eV.

Calorimetric energy measurements have been used by a number of experimentalists in measuring the energy losses and heat dissipation resulting from the passage of radiation through matter. Although the

---

[7] F. Kalil, W. G. Stone, H. H. Hubbell, Jr., and R. D. Birkhoff, "Stopping Power of Thin Aluminum Foils for 12 to 127 Kev Electrons", ORNL-2731, Oak Ridge National Laboratory, Oak Ridge, Tennessee. Unpublished.

[8] F. Seitz and J. S. Koehler, SOLID STATE PHYSICS (Academic Press, New York, 1956), Volume 2, p. 309.

purpose of these early workers was not to measure stopping power, it is worthwhile to examine their methods and techniques.

Calorimetric techniques for measuring the heating effects of ionizing radiations were first used by Curie and Laborde[9] when they showed that radium maintained a higher temperature than its surroundings. This effect was measured in a Bunsen ice calorimeter. Rutherford and Barnes[10] then showed that this heating effect was closely connected with the α activities of the various daughter products. It seemed probable that the heating due to individual products in equilibrium should be proportional to the energy of the α-particle emitted. Rutherford and Robinson[11] tested this hypothesis by studying the heating effects of radon and its products. Platinum wire coils were wound on identical glass tubes and formed two arms of a Wheatstone bridge. A galvanometer was used to measure the balance upset when a radon tube was placed inside one of the coils. The radon tube was connected by capillary tubes and stopcocks to a pumping system. This allowed introduction and removal of the radon gas at proper times so that the heating effects of radium A, B, and C could be distinguished. The system was calibrated by passing a known current through a coil of manganin wire which replaced the source and occupied the same volume. When allowance was made for heating due to beta and gamma rays (estimated to be about

---

[9] P. Curie and A. Laborde, Comp. Rend., 136, 673 (1903).

[10] E. Rutherford and H. Barnes, Phil. Mag., 7, 202 (1904).

[11] E. Rutherford and H. Robinson, Phil. Mag., 25, 312 (1913).

four per cent), Rutherford and Robinson found the observed heating to be in good agreement with the values calculated from α energies.

In subsequent experiments, Watson and Henderson[12] made careful measurements of the heating effects of several radioactive products by a resistance thermometer method similar in principle to that employed by Rutherford and Robinson, and found in all cases that the heating of the products was proportional to the energy of the emitted α particles.

The beta-particle spectra has been important in nuclear physics, especially with regard to the balance of energy in nuclear equations. Calorimetric energy determinations played an important part in resolving the problem of the continuous beta spectrum.

When it was first observed that beta particles seemed to be emitted with a spectrum of energies, several interpretations of this phenomenon were set forth. Rutherford's[13] explanation was that a beta particle was expelled from the nucleus with a definite energy but lost part of this energy by exciting characteristic radiation, such as gamma and/or secondary beta radiation, before leaving the atom. He contended that the combined energies of the radiations should represent the energy of the original beta particles. Calculations by Moseley and Robinson[14] using the heating effects of radium C showed the combined energy of Ra C to be 3.02×10^{-6} erg. This, according to Rutherford's theory, should not be less than the energy of the most energetic beta particle emitted. But Rutherford and Robinson[15] had previously found betas from Ra C with energies as high as 3.9×10^{-6} ergs.

---

[12] S. W. Watson and M. C. Henderson, Proc. Roy. Soc., A-118, 318 (1928).

[13] E. Rutherford and H. Robinson, op. cit.

[14] H. G. Moseley and H. Robinson, Phil. Mag., 28, 327 (1914).

[15] E. Rutherford and H. Robinson, op. cit.

Thus the results of the experiment were at variance with the existing theory. The problem seemed to hinge on the question as to whether or not the observed spectrum of beta particles was due to secondary processes or due to a continuous energy spectrum when emitted from the nucleus. If the continuous spectrum is a result of secondary processes, then the average energy of each disintegration should equal E_{max}. If, on the other hand, the beta particles are actually emitted with various energies, the average energy of disintegration should correspond to the mean energy of the continuous spectrum. To decide between these views, it was necessary to measure the total energy of disintegration of a beta-emitter whose spectrum was known.

The average energy of beta particles of a continuous spectrum can be calculated from an energy distribution curve. If T_o is the end point energy, then the average energy is given by

$$\bar{T} = \frac{\int_0^{T_o} N(T)T\,dT}{\int_0^{T_o} N(T)\,dT} , \qquad (2)$$

where the numerator is the total energy found by integrating the product of the number of particles per unit energy of a given energy and that energy; and the denominator is the total number of particles emitted irrespective of energy. The number of particles is equal to the area under the energy distribution curve.

The average energy associated with a disintegration can be found experimentally by a direct calorimetric measurement of the heat energy produced by a known number of disintegrations. The literature describes

several successful experiments of this kind where the beta-emitter was placed inside a calorimeter designed to absorb all disintegration products. Ellis and Wooster[16], using the beta-emitter Radium E obtained values of 0.35 ± 0.04 Mev as the average energy, in good agreement with the mean energy value of 0.39 Mev obtained directly from the energy distribution curve. Their method was as follows: RaE was deposited on either a short platinum or nickel wire and enclosed in a thin brass case. This could be lowered into a tubular lead calorimeter of thickness such that all beta rays would be absorbed. An identical calorimeter with a dummy non-activated wire gave symmetry to eliminate external disturbances. The two calorimeters, with connecting thermocouples, were enclosed in a massive copper block. The steady temperature difference between the calorimeters was measured by thermocouples which were attached to a sensitive galvanometer. The heating effect was studied several days, and from the activity of the radium E that remained at any time and the Ra F that had grown, the effect of Ra E beta rays alone was deduced. By relating the heat dissipated to the number of particles decayed, they showed that the heat corresponded to the mean energy rather than the end-point energy. Meitner and Orthmann[17] likewise performed calorimetric energy measurements, obtaining a value of 0.337 ± 0.020 Mev. More recently, Neary[18] obtained a value of 0.340 Mev in a similar experiment. In the work done by Meitner and Orthmann, the average energy of the

---

[16] C. D. Ellis and B. A. Wooster, Proc. Roy. Soc., A-117, 109 (1928).

[17] L. Meitner and W. Orthmann, Zeit. f. Physik, 60, 143 (1930).

[18] G. J. Neary, Proc. Roy. Soc. (London), A-175, 71 (1940).

primary beta particles of radium E was measured. A differential calorimeter was used which consisted of two identical cylindrical calorimeters one centimeter in diameter. A source (radium E) was inserted in one calorimeter, and a constantan heating coil was used to heat the other. The two calorimeters were placed in an evacuated glass jar surrounded by a copper insulating pot. This was all suspended in a Dewar flask filled with water and held at a constant temperature. Fifteen sets of thermocouples were used to measure the temperature difference between calorimeters, each having one junction in the source calorimeter and the other junction in the "dummy" calorimeter. A null method was used in which the heating from the source was balanced by the heat from the constantan heating coil. The galvanometer used as a null detector had a sensitivity such that a heating difference of 5.5×10^{-8} watts gave a deflection of 1 millimeter. The heat leakage losses of the system were by radiation and donduction in the thermopile wires. Because these early calorimetric measurements showed that the average energy per disintegration did correspond to the mean energy, it was evident that a spectrum of energies did exist. This in turn led to our present theory of beta decay and the neutrino hypothesis.

Meanwhile, in 1925, Gurney[19] studied beta spectra of radium B and radium C and calculated the expected heating effect of this decay. His value of 5.6 cal hr^{-1} gm^{-1} agreed reasonably well with the 4.7 cal/hr as found experimentally by Rutherford and Robinson[20]. A good part of the

---

[19] R. W. Gurney, Proc. Roy. Soc., A-109, 540 (1925).

[20] E. Rutherford and H. Robinson, op. cit.

discrepancy may be attributed to the fact that Rutherford was actually using data from experiments on the heating of alpha particles and simply found the effect of betas by subtracting.

By 1950 calorimetric methods and techniques were further advanced by the introduction of thermistors -- thermally sensitive resistors. Laughlin and Beattie[21] were successful in using thermistors in a calorimetric determination of the energy flux of 22.5 Mev X-rays. The method was simply to imbed thermistors in the irradiated material, which was used as a calorimeter. These energy values were then related to cavity ionization measurements so that the result could be given in $\frac{\text{erg}}{\text{cm}^2\text{-roentgen}}$. Their method was to suspend in a calorimeter two identical lead cylinders each containing a Western Electric 3,000 ohm thermistor. These thermistors constituted opposing arms of a Wheatstone bridge. A sensitive galvanometer was used to detect bridge current when the system was irradiated with X-rays. The system was calibrated by using constantan wire heating coils in each cylinder. Knowing the amount of energy dissipated by the coils, the X-ray energy was determined by producing the same bridge resistance change in the same time interval.

Laughlin and Beattie continued their work and in 1953 described[22] further studies in the evaluation of the roentgen for 400 Kev and 22.5 Mev X-rays. They obtained greater sensitivity by use of a special amplifier

---

[21] J. S. Laughlin and J. W. Beattie, Rev. Sci. Inst. 22, 572 (1951).

[22] J. S. Laughlin and J. W. Beattie, Am. J. Roent., 70, 294 (1953).

instead of a galvanometer as the null detector for the Wheatstone bridge. In 1955 Johns, Bernier, and Cormack[23] described a method for measuring directly with thermistors the energy locally absorbed from a gamma-ray beam.

The reason for discussing these early works is to point out the usefulness and realiability of calorimetric measurements of the energy imparted to matter by radiation. In principle, one wishes to make precisely the same sort of determination to measure stopping power. The techniques and methods were, of course, quite different, but in effect the problem was approached in the same manner. Such measurements can then be related to Bethe's stopping theory and serve to bring about a better understanding of the stopping power phenomenon.

O. E. Meyers[24], in his review of the development of instruments and techniques used in calorimetric radioactivity measurements, discusses several important considerations for work of this type. He states: (1) a constant room temperature is desirable with no variations greater than 0.5°C; (2) the calorimeter should be housed in a vessel whose temperature is controlled to within 0.001°C. It is desirable that the temperature be slightly above room temperature; (3) the calorimeter should have a low-heat capacity and be thermally insulated from the enclosing vessel; (4) conduction losses should be minimized by making a minimum number of electrical

---

[23] H. E. Johns, J. P. Bernier, and D. V. Cormack, Nature, 176, 560 (1955).
[24] O. E. Meyers, Nucleonics, 5, No. 5, 37 (1949).

connections and using small gauge wires; (5) conduction and convection losses may be reduced by evacuating the jacket of the system. These suggestions were followed as much as possible in the apparatus and techniques described herein.

In this work, stopping power measurements were made for a 191.8 microgram per square centimeter copper foil bombarded by monoenergetic electrons whose energies varied from 31.56 to 126.56 Kev. Monoenergetic electrons from an electron gun were accelerated by a linear accelerator and impinged normally on the foil. The power dissipated as heat in the foil by the transmitted beam was measured calorimetrically using copper-constantan thermocouples. The power divided by the current of the electron beam passing through the foil gave the average energy loss $\overline{\Delta E}$ directly. The path length, which corresponded to the foil thickness, was obtained by weighing a known area of foil. This thickness, given in micrograms per square centimeter, was corrected for scattering effects to give the true path length, $\overline{\Delta x}$. The stopping power was then given by the ratio $\overline{\Delta E}/\overline{\Delta x}$.

II. THEORY

A. Stopping Power

The theory of stopping power has been reviewed recently by Bethe and Ashkin[25] and by Birkhoff[26] and only the conclusions are stated here.

Using the Möller formula for the electron-electron scattering cross section, Bethe's expression for electron stopping power is given by

$$-\frac{dE}{dx} = \frac{2\pi N_A e^4 \rho Z}{m_o v^2 A}\left[\ln \frac{m_o v^2 E}{2I^2\gamma^2} - (2\gamma - \gamma^2)\ln 2 + \gamma^2 + \frac{1}{8}(1-\gamma)^2\right] \qquad (3)$$

where N_A = Avogadro's Number

ρ = Density of the Material

Z = Atomic Number of the Material

A = Atomic Weight of the Material

m_o = Electron Rest Mass

v = Velocity of Bombarding Electron

e = Electron Charge

E = Kinetic Energy of the Electrons (total energy - rest mass energy)

I = Mean Excitation Potential $\approx 13.5Z$

$\gamma = \sqrt{1 - v^2/c^2}$ where c is velocity of light

---

[25] H. A. Bethe, and J. Ashkin, PASSAGE OF RADIATIONS THROUGH MATTER. EXPERIMENTAL NUCLEAR PHYSICS, (Edited by E. Segre, Wiley and Sons, New York, 1953) Volume I, pp. 166-367.

[26] R. D. Birkhoff, op. cit.

This expression correctly gives the average rate of energy loss provided the following are true:

(1) The energy of the impinging electron is much greater than the binding energies of the atomic electrons.

(2) The energy is low enough so that no correction for density effect is required.

(3) The energy losses by radiation are small.

In this work, all of the above were true for the energy range considered (~ 30 to 130 Kev incident electron energy).

B. Calorimetry

1. The Fundamental Heat Equation

Consider a system of mass m and specific heat c consisting of a metallic foil and its support ring. Using a set of thermocouples, one wishes to determine the heat energy dissipated in the foil by a beam of electrons impinging normally upon the foil. For reasons which will become apparent, it is convenient to add a second set of thermocouples to be used for cooling the system by the Peltier effect. The following factors then contribute to the heating and cooling of the system:

(1) Beam heating, caused by energy dissipated in the foil by the passage of electrons;

(2) Peltier heating or cooling depending on direction of thermocouple current;

(3) Joule or i_P^2R heating, resulting from currents in the Peltier thermocouple wires;

(4) Heat leakage between the system and its environment.

Thus one may describe the system by

$$(i_B\overline{\Delta E}) + \left[n\pi T\ i_P + \frac{1}{2}\ i_P^2 R\right] + L(T_o - T) = mcJ\dot{T} \qquad (4)$$

where i_B = Beam current

$\overline{\Delta E}$ = Energy loss in foil

n = Number of thermocouples in Peltier set

π = Thermoelectric power for copper-constantan thermocouple

i_P = Peltier current

R = Resistance in Peltier thermopile

$L(T_o-T)$ = Heat leakage when system is at temperature T and the environment at temperature T_o

m = Mass of system

c = Specific heat of system

J = Mechanical equivalent of heat

$\dot{T}$ = Rate of temperature change of foil

Equation (4) suggests two possible modes of operation for determining the net heating of the system due to the electron beam. In the drift method, let $i_P = 0$ and evaluate $\dot{T}$ at $T = T_o$. Then

$$\overline{\Delta E} = \frac{mcJ\dot{T}}{i_B} \qquad (5)$$

In the null method, let $\dot{T} = 0$ and $T = T_o$. Then

$$\overline{\Delta E} = \frac{-(n\pi T i_P + \frac{1}{2} i_P^2 R)}{i_B} . \tag{6}$$

The drift method was chosen for this work because more reproducible results were obtained with it. Both methods will be discussed, however, and the relationship between the two will be pointed out.

2. The Drift Method

(a) Equation for the Power Loss in the Foil

For the drift method,

$$i_B\overline{\Delta E} = mcJ\dot{T} \tag{7}$$

where $i_B\overline{\Delta E}$ is the power in watts. For the more general case when $T \neq T_o$:

$$i_B\overline{\Delta E} = mcJ\dot{T} - L(T_o - T) \tag{8}$$

Equation (8) may be solved for $\dot{T}$ and yields

$$\dot{T} = \left(\frac{1}{mcJ}\right) i_B\overline{\Delta E} + \left(\frac{L}{mcJ}\right)(T_o - T) \tag{9}$$

or more simply

$$\dot{T} = K_1 i_B\overline{\Delta E} + K_2(T_o - T) \quad , \tag{10}$$

where K_1 is a calibration constant and K_2 is the heat loss constant.

Assuming that at time $t = 0$ the system is at temperature T_i then one wishes to know the temperature T at any time t. To solve for T in Equation (10), the variables may be separated and both sides of the equation may be integrated:

$$\int_{T_i}^{T} \frac{dT}{K_1 i_B \overline{\Delta E} + K_2(T_o - T)} = \int_{o}^{t} dt \tag{11}$$

or

$$t = -\frac{1}{K_2} \ln \left[\frac{K_1 i_B \overline{\Delta E} + K_2 (T_o - T)}{K_1 i_B \overline{\Delta E} + K_2 (T_o - T_i)} \right] . \tag{12}$$

The solution for T is:

$$T = \left[\frac{K_1}{K_2} i_B \overline{\Delta E} + T_o \right] \left[1 - e^{-K_2 t} \right] + T_i e^{-K_2 t} . \tag{13}$$

The slope may be evaluated if one defines T_+ at time $t_+ = t_o + \Delta t$ and T_- at time $t = t_o - \Delta t$. Then

$$\dot{T} = \frac{T_+ - T_-}{t_+ - t_-} = \frac{\left[\frac{K_1}{K_2} i_B \overline{\Delta E} + T_o \right] \left[-e^{-K_2(t_o + \Delta t)} + e^{-K_2(t_o - \Delta t)} \right] - \left[T_i \right] \left[-e^{-K_2(t_o + \Delta t)} + e^{-K_2(t_o - \Delta t)} \right]}{2 \Delta t}$$

$$= \frac{\left[\frac{K_1}{K_2} i_B \Delta E + T_o - T_i \right] \left[(e^{-K_2 t_o}) \left(-e^{+K_2 \Delta t} - e^{-K_2 \Delta t} \right) \right]}{2 \Delta t} . \tag{14}$$

This may be written

$$\dot{T} = \frac{e^{-K_2 t_o}}{\Delta t} \left[\frac{K_1}{K_2} \, i_B \overline{\Delta E} + T_o - T_i \right] \sinh K_2 \, \Delta t \quad . \tag{15}$$

From Equation (12), t_o is just

$$t_o = - \frac{1}{K_2} \ln \frac{K_1 i_B \overline{\Delta E}}{K_1 i_B \overline{\Delta E} + K_2 (T_o - T_i)} \quad . \tag{16}$$

Then,

$$\dot{T} = \frac{K_1 i_B \overline{\Delta E}}{K_1 i_B \overline{\Delta E} + K_2 (T_o - T_i)} \; \frac{\left(\frac{K_1}{K_2} i_B \overline{\Delta E} + T_o - T_i \right)}{\Delta t} \sinh K_2 \Delta t \; . \tag{17}$$

Simplifying

$$\dot{T} = \frac{K_1}{K_2} \, i_B \overline{\Delta E} \left(\frac{\sinh K_2 \Delta t}{\Delta t} \right) \tag{18}$$

The power delivered to the foil is then

$$i_B \overline{\Delta E} = \frac{1}{K_1} \, \dot{T} \left(\frac{K_2 \Delta t}{\sinh K_2 \Delta t} \right) \tag{19}$$

(b) Theoretical Determinations of Heat Loss Constant K_2

K_2 may be computed from theoretical considerations as follows. From Equations (9) and (10) it is seen that

$$K_2 = L/mcJ \tag{20}$$

Now L is just the coefficient of the heat leakage term in Equation (4). If one assumes that no heat losses by radiation were involved, then in accordance with the usual definition of coefficient of heat conductivity k,

$$L = k(A/\ell) \quad . \tag{21}$$

Where A is the cross sectional area and ℓ the length of the system.

Heat conduction losses were almost entirely through the thermocouple wires. There were a total of twelve sets of copper-constantan thermocouples or a total of 24 wires. In addition, there was another copper wire which was used in measuring the foil current. Then, the conduction loss through the copper wires was

$$L_{copper} = \frac{n\, k_{cu}\, A_{cu}}{\ell_{cu}} \tag{22}$$

where n is the number of wires (=13); k_{cu} is the heat conductivity = 0.918 cal/sec $cm^2 K°$; A = 0.00501 mm^2 for No. 40 Cu wire; ℓ = 2 cm.

Similarly, for constantan,

$$L_{con} = \frac{n\, k_{con}\, A_{con}}{\ell_{con}} \tag{23}$$

where n = 12; k = 0.054 cal/sec $cm^2 K°$; A = 0.007967 mm^2 for No. 38 constantan; ℓ = 2 cm. Using these values the total heat loss coefficient is

$$L_{total} = L_{cu} + L_{con} = 13.65 \times 10^{-4} \ \frac{\text{watt}}{K°} \tag{24}$$

The value (mc) must now be calculated from Equation (20). This value includes the mc values of the foil, its copper support ring, and the plastic ring holder. The foil weight is negligible compared to that of the rest of the system, so that

$$mc_{total} = (mc)_{copper} + (mc)_{plastic} \quad . \tag{25}$$

For the copper ring, m = 0.875 gm and c = 0.0921 cal/cm°K and for the plastic holder m = 0.190 gm and c = 0.25 cal/cm°K. Using these values we obtain $mc = \Sigma m_i c_i = \left[(0.875)(0.0921)\right] + \left[\ .190 \times .25\ \right] = .1281$ cal/°K for the system. Therefore the calculated value of K_2 was

$$K_2 = \frac{L}{mcJ} = 0.152 \text{ min}^{-1} \tag{26}$$

where J is the mechanical equivalent of heat.

(c) Theoretical Determination of Calibration Constant K_1

If heat loss is neglected by evaluating $\dot{T}$ at $T \cong T_o$, then

$$\dot{T} = K_1 i_B \overline{\Delta E} \tag{27}$$

where $\dot{T}$ has units of K°/sec, i_B is in amperes, $\overline{\Delta E}$ is in volts, and K_1 is a calibration constant with dimensions of K°/joule. It has been shown that $K_1 = \frac{1}{mcJ}$ and that mc = 0.1281 cal/K°. It follows that K_1 = 1.86 K°/joule.

The rate of heating, $\dot{T}$, was determined from the rate of deflection of a sensitive galvanometer which measured the voltage developed in the temperature monitoring thermopile. The above equation may be written in terms of the rate of galvanometer deflection to give

$$\alpha \dot{D} = K_1 i_B \overline{\Delta E} \tag{28}$$

where α is the constant of proportionality relating $\dot{T}$ and $\dot{D}$. The constants α and K_1 may be combined as a single constant giving

$$i_B \overline{\Delta E} = C_1 \dot{D} \tag{29}$$

where C_1 is just α/K_1 or $C_1 = \alpha mcJ$.

To determine the value of C_1 it is necessary to evaluate α for the system. The temperature monitoring thermopile and galvanometer may be represented by the equivalent circuit shown in Figure (1). The thermopile consisted of six copper-constantan thermocouples for a total EMF of 240 $\mu v/K^\circ$. The pile resistance was 8.0 ohms. The galvanometer, whose internal resistance was 14.3 ohms and sensitivity 0.050 $\mu v/mm$, completed the circuit. Therefore, the voltage drop across the galvanometer was

$$V_G = \left(\frac{14.3}{14.3 + 8} \right) 240 = 153.6 \ \frac{\mu v}{K^\circ} \tag{30}$$

UNCLASSIFIED
ORNL-LR-DWG. 37874

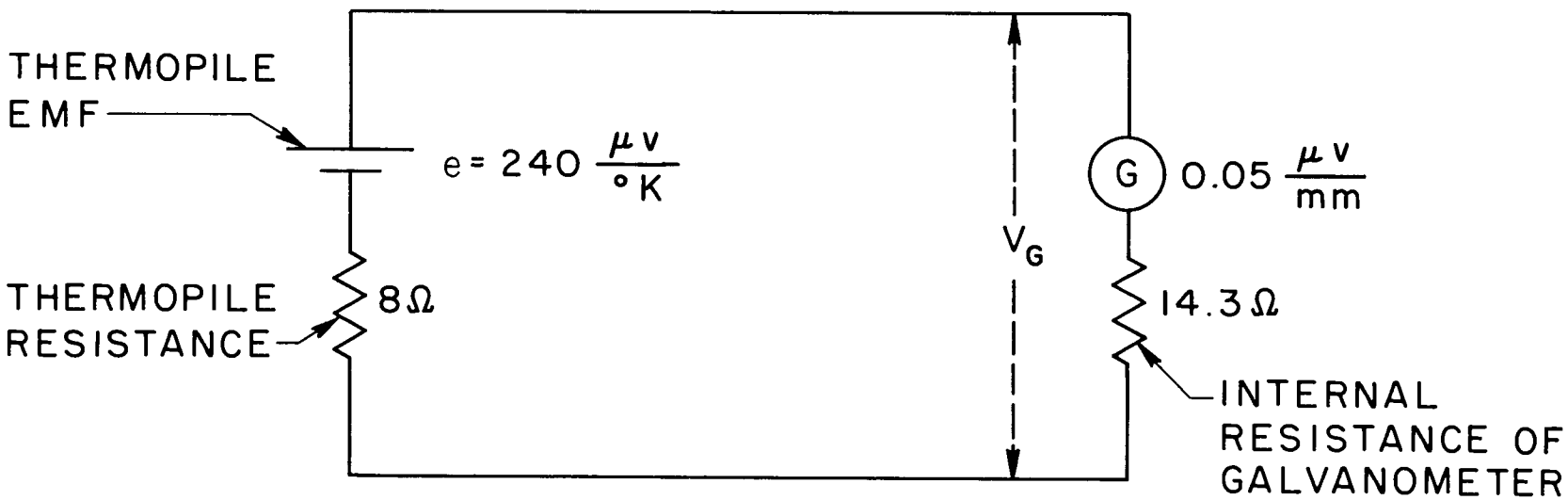

Fig. 1. Equivalent Circuit for Temperature Monitoring Thermopile.

Using the galvanometer sensitivity of 0.050 μv/mm and the voltage drop across the galvanometer of 153.6 μv/K° it may be seen that

$$\alpha = .05\ \mu v/mm \times \frac{1}{153.6}\ \mu v/K^{\circ} \times \frac{10\ mm}{cm} \tag{31}$$

$$= 3.25\ 10^{-3}\ K^{\circ}/cm$$

Using this value gives

$$C_1 = 29.2\ \frac{\mu\ watt}{cm/min} \tag{32}$$

For convenience, C_1 was used as the actual calibration constant of the system. Had K_1 been used, the proportionality factor, α, would have to be used each time to relate K_1 to the galvanometer drift.

3. The Null Method

An important effect of electric currents in metallic conductors is the reversible thermoelectric effect known as the Peltier effect. When an electric current is maintained across the junction of two dissimilar metals, as in a thermocouple, the junction temperature changes unless heat is supplied or removed externally. It is quite

clear that this effect is a means of heating or cooling the vicinity of such a junction. The rate at which heat must be supplied to the junction to maintain its temperature depends only on the amount and sign of the current passing through the junction, that is, heat is supplied to the junction at a rate proportional to the current, and when the current is reversed, heat is removed from the junction.

The fact that the heat must be added or removed from a thermocouple junction to keep its temperature constant suggests that an EMF exists between the metals, and this is actually the case. For a given thermocouple, the EMF is generally a function of temperature T so that heat must be supplied when a charge q is transported across the junction. If we denote the Peltier EMF by π(volts/K°), then the heat supplied to the junction must equal πqT joules.

It should be emphasized that Joule heating always occurs in addition to the Peltier effect when a current passes through a thermocouple junction. Thin means that the total effect is the sum of two, $(i_P^2 Rt + \pi qT)$ joules, where t denotes time. The $i_P^2 Rt$ term is, of course, independent of the direction of the current, while the πqT term heats for the current in one direction and cools in the other. Thus one can only use a thermocouple for cooling when the πqT term is negative and is greater than $i_P^2 Rt$. As shown by the curve in Figure (2), there will be two regions where

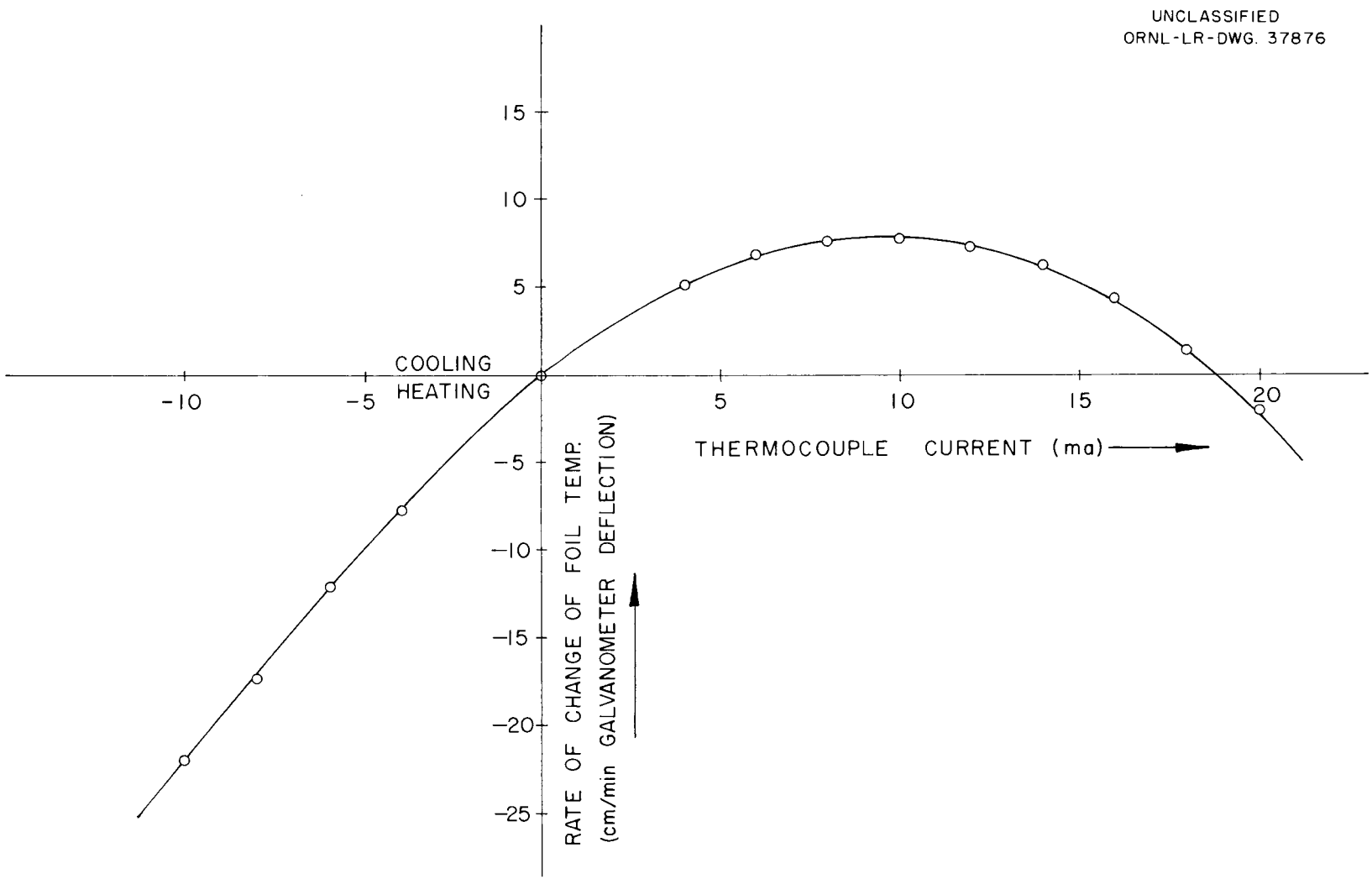

Fig. 2. Use of Peltier Effect for Cooling Foil.

the net effect is heating. One, of course, is where the πqT is positive as heating, and the other where the Joule heating is greater than the $-\pi qT$ cooling. In Figure (2) the rate of temperature change of the foil (in cm/min on the temperature monitoring galvanometer) is plotted as a function of cooling current through the cooling thermopile. For convenience, the curve is plotted with cooling current in the positive direction on the abscissa.

Only half the Joule heat developed in the thermocouples contributes to the heating of the system*. The other half is dissipated at the opposite reference junction (i.e., the environment). If the net Peltier effect is always taken to include the associated i_P^2R heating, the system experiences a net Peltier heating (or cooling) of $[\pi qT + \frac{1}{2} i_P^2Rt]$ joules. In terms of power, we may write

$$P = (n\pi T) \quad i_P + \frac{1}{2} \quad i_P^2R \tag{33}$$

for n thermocouples where R is the sum of the resistances of all the thermocouples and i_P is the current through the thermocouples.

---

* See Appendix I.

In the null method, the beam heating was canceled out by cooling the foil by the Peltier effect. If this was done at $T = T_o$, then

$$(i_B \overline{\Delta E}) = -(n\pi T\, i_P + 1/2\, i_P^2 R) \tag{34}$$

The experimental curve of Figure (2) can be checked by Equation (33). Using $\pi = 40\ \mu v/K^\circ$ for a copper-constantan thermocouple, we have $n\pi = 240\ \mu v/K^\circ$ for a six-couple thermopile. Total resistance was 8 ohms; absolute temperature of the system was 302 K°. Using these values in the equation, it may be shown that $P = 0$ when $i_P = 0$ and when $i_P = 18.12$ ma. These values are in agreement with the experimental values as plotted on the curve. Furthermore, taking the first derivative with respect to i_P we have

$$\frac{dP}{di_P} = (n\pi T) + i_P R \tag{35}$$

Then $dP/di_P = 0$ when $i_P = 9.06$ ma which agrees again with the experimental value.

4. Relation Between the Drift Method and the Null Method

It was stated earlier that the two methods of operating the system were: the drift method where $i_B \overline{\Delta E} = mc\dot{T}$; and the null method where $n\pi T i_P + 1/2(i_P^2 R) + i_B \overline{\Delta E} = 0$. The two methods are related by the beam

power, $i_B \overline{\Delta E}$ which may be made the same for both. Thus

$$n\pi T i_p + 1/2\,(i_p^2 R) = -mcJ\dot{T} = -mc\,\alpha\,\dot{D} = -C_1\,\dot{D} \qquad (36)$$

Or

$$C_1 = \frac{n\pi T\; i_p + 1/2\,(i_p^2 R)}{-\dot{D}} \qquad (37)$$

This value of $\dot{D}$ is chosen from Figure (2) corresponding to the i_p used in the above. The calibration constant, C_1, should be the same as that calculated previously by the drift method alone.

C. Nuclear Scattering Effects

1. Single Scattering and Extraneous Heating

Single scattering of primary electrons by the nuclei of the absorber becomes a matter of some concern in high Z materials. In the case of a metallic foil target with copper mounting ring, any primaries scattered into the small solid angle subtended by the copper ring will lose all their energy in the ring and provide extraneous heating to the system. Although the number of electrons scattered in this direction is small (usually less than one per cent) the fact that they dissipate all their energy makes them significant. The effect is about the same as if a small fraction of the incident beam struck the ring directly rather than only the foil. One may calculate from single scattering theory the probability of an electron scattering into the solid angle subtended by the ring.

Rutherford[27] in his treatment of single nuclear scattering showed that for high energy electrons the differential cross section for scattering through an angle between θ and $\theta + d\theta$ into a solid angle $d\Omega = 2\pi \sin\theta\, d\theta$ is

$$d\Phi(\theta) = \left[\frac{\pi Z^2 e^4 (1-\beta^2)}{2 m_o^2 v^4} \right] \frac{\sin\theta d\theta}{\sin^4(\theta/2)} \tag{38}$$

where Z is the atomic number of foil, v and m_o are the electron velocity and mass, $\beta = v/c$, and e is the electronic charge. This may be integrated between the limits of θ_1 and θ_2 to give:

$$\int_{\theta_1}^{\theta_2} d\Phi(\theta) = \frac{\pi Z^2 e^4 (1-\beta^2)}{m_o^2 v^4} \left[\frac{1}{\sin^2(\theta_1/2)} - \frac{1}{\sin^2(\theta_2/2)} \right] \tag{39}$$

If the number of atoms per cubic centimeter is given by $N = \frac{N_a \rho}{A}$, then the total probability for scattering into the angular increment between θ_1 and θ_2 is

$$\frac{N_A \rho}{A} t \int_{\theta_1}^{\theta_2} d\Phi(\theta).$$

The more exact single scattering cross section obtained by Mott[28] in the form of an infinite series has been evaluated recently on the digital computer by Doggett and Spencer.[29] These results are given as a ratio of

---

[27] E. Rutherford, Phil. Mag. 21, 669 (1911); also R. D. Birkhoff, op. cit.

[28] N. F. Mott, Proc. Roy. Soc. Lond., A-124, 425 (1929); A-135, 429 (1932).

[29] J. A. Doggett and L. V. Spencer, Phys. Rev. 103, 1597 (1956).

the Mott to the Rutherford cross sections, σ/σ_R. For a given energy and atomic number, the ratio changes only slowly over the angular range between θ_1 and θ_2 and an average value of the ratio may be used with little error. Thus the fraction f of the incident electron beam which strikes the ring is

$$f = (\overline{\sigma/\sigma_R}) \frac{N_A \rho}{A} t \frac{\pi Z^2 e^4 (1-\beta^2)}{m_o^2 v^4} \left[\frac{1}{\sin^2 (\theta_1/2)} - \frac{1}{\sin^2 (\theta_2/2)} \right] \quad (40)$$

A typical range of values for Spencer's* ratio is shown in Figure (3) for $\theta = 101°$. The ratio σ/σ_R was plotted as a function of the atomic number for various incident electron energies.

The geometry of the mounting ring in relation to the incident beam is shown in Figure (4). In both cases (a) and (b) the ring subtends an angle of 22° at the center of the foil. Scattering into the ring was less in case (a), because the scattering angle was greater than 90°. For this reason, case (a) geometry was used in mounting the foils.

The effect of single scatter on the experimentally determined stopping power may be calculated as follows. Assume the heating H of the foil due to the electron beam is

$$H_{exp} = i_B \left(-\frac{dE}{dx} \right)_{exp} t \quad (41)$$

where i_B is the beam current, $\left(-\frac{dE}{dx} \right)_{exp}$ the stopping power of the foil to be determined experimentally, and t the foil thickness.

---

* The values used in Figure (3) were interpolated from the tables of Spencer and Doggett. The angle $\theta = 101°$ represents the average angle of scatter into the mounting ring (see Figure 4).

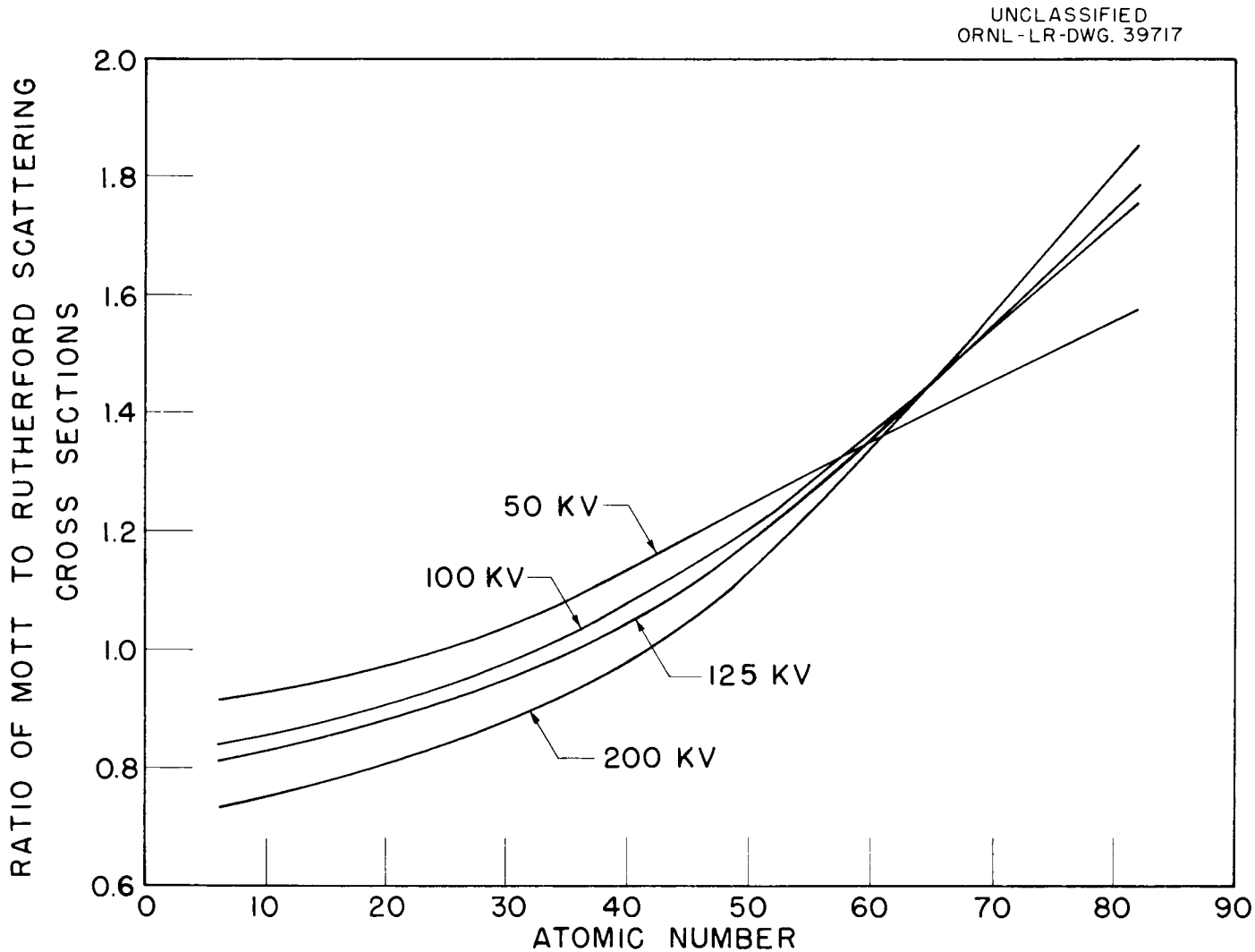

Fig. 3. Spencer's Ratio for $\theta = 101°$.

UNCLASSIFIED
ORNL-LR-DWG. 37875

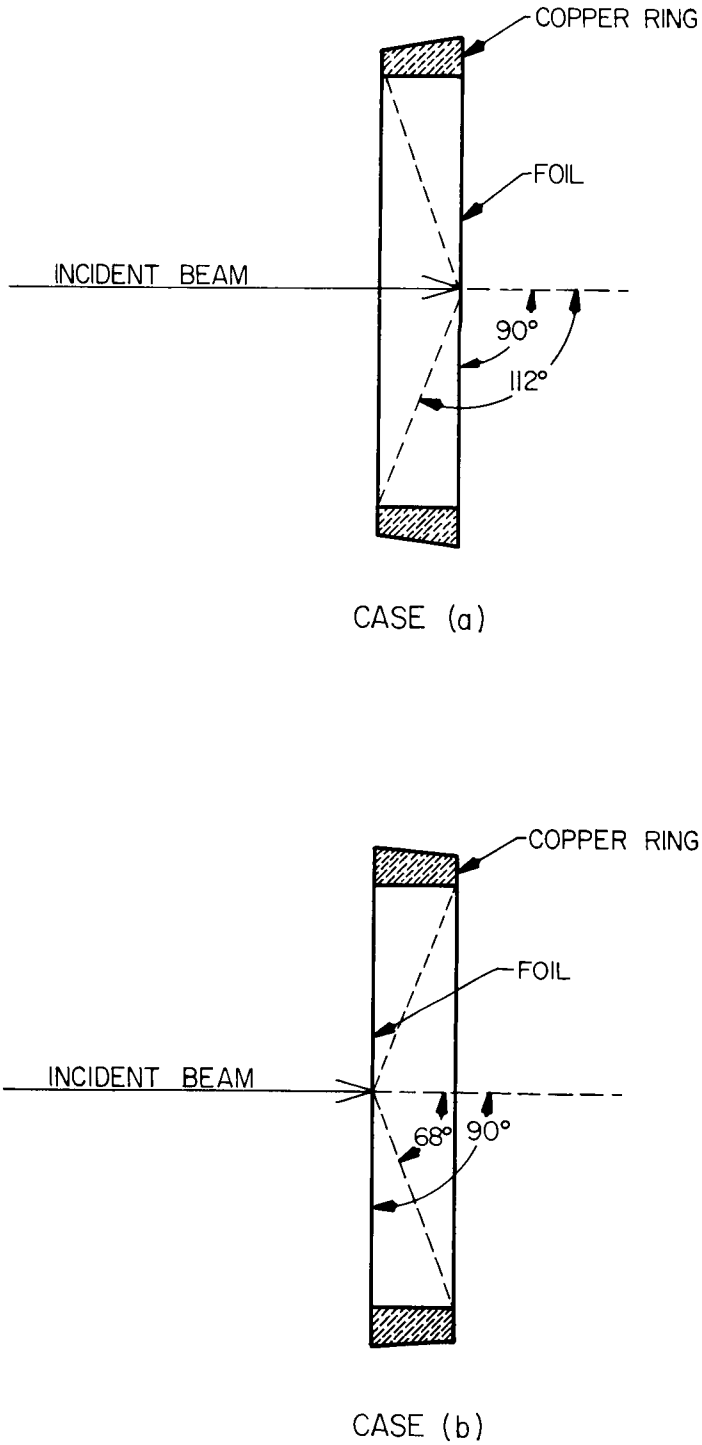

Fig. 4. Single Scattering of Primary Electrons into Foil Mounting Ring.

Due to single scattering into the support ring, the apparent heating is

$$H_{app} = H_{exp}(1-f) + i_B Ef \tag{42}$$

Or

$$i_B \left(\frac{dE}{dx} \right)_{app} t = i_B \left(\frac{dE}{dx} \right)_{exp} t(1-f) + i_B Ef \tag{43}$$

where $i_B Ef$ is heating in the ring when a fraction f of the beam strikes the support ring. Equation (44) may be written

$$-(1-f) \left(\frac{dE}{dx} \right)_{exp} + \left(\frac{dE}{dx} \right)_{app} = \frac{fE}{t} \tag{44}$$

Replacing $\frac{dE}{dx}$ by $\frac{\overline{\Delta E}}{t}$:

$$-(1-f) \left(\frac{\overline{\Delta E}}{t} \right)_{exp} + \left(\frac{\overline{\Delta E}}{t} \right)_{app} = \frac{fE}{t} \tag{45}$$

or since t is the same in all cases

$$-(1-f)\, \overline{\Delta E}_{exp} + \overline{\Delta E}_{app} = fE \tag{46}$$

Solving for $\overline{\Delta E}_{exp}$:

$$\overline{\Delta E}_{exp} = \frac{(\overline{\Delta E})_{app} - fE}{1-f} \tag{47}$$

Finally we may say that for a given energy E

$$\frac{\overline{\Delta E}_{app}}{E} = (1-f) \frac{\overline{\Delta E}_{exp}}{E} + f \tag{48}$$

In Figure (5) $\Delta E_{app}/E$ is plotted as a function of f for several values of $\Delta E_{exp}/E$. If one sets the criterion that no more than half the apparent heat loss may occur in the copper ring, then a limit on usable data is established by setting the foil heating equal to the ring heating. That is

$$(1-f)\ \overline{\Delta E}_{exp} = fE \tag{49}$$

This boundary is indicated also in Figure (5). Only values to the left of the boundary line are considered valid. If for a given run, a value to the right of the boundary was obtained, data were discarded and a new run made using different energy and /or foil.

In the case of the copper foil, the amount of scattering into the support ring and bias discs was so small that the effect was not detectable as current on the foil and bias galvanometers. Calculations showed that indeed less than 1% of the incident beam current could be expected to strike the ring in most cases.

Single scattering effects could be detected as current to the ring and discs, however, for materials of higher Z such as gold. Figure (6) shows the behavior of the bias disc current as a function of cup current for various beam energies. It is seen that for low incident energies more bias current appears. Furthermore, as the cup current is increased, the bias current also increases. These data were obtained using a 201.6 $\mu g/cm^2$ gold

UNCLASSIFIED
ORNL-LR-DWG. 39718

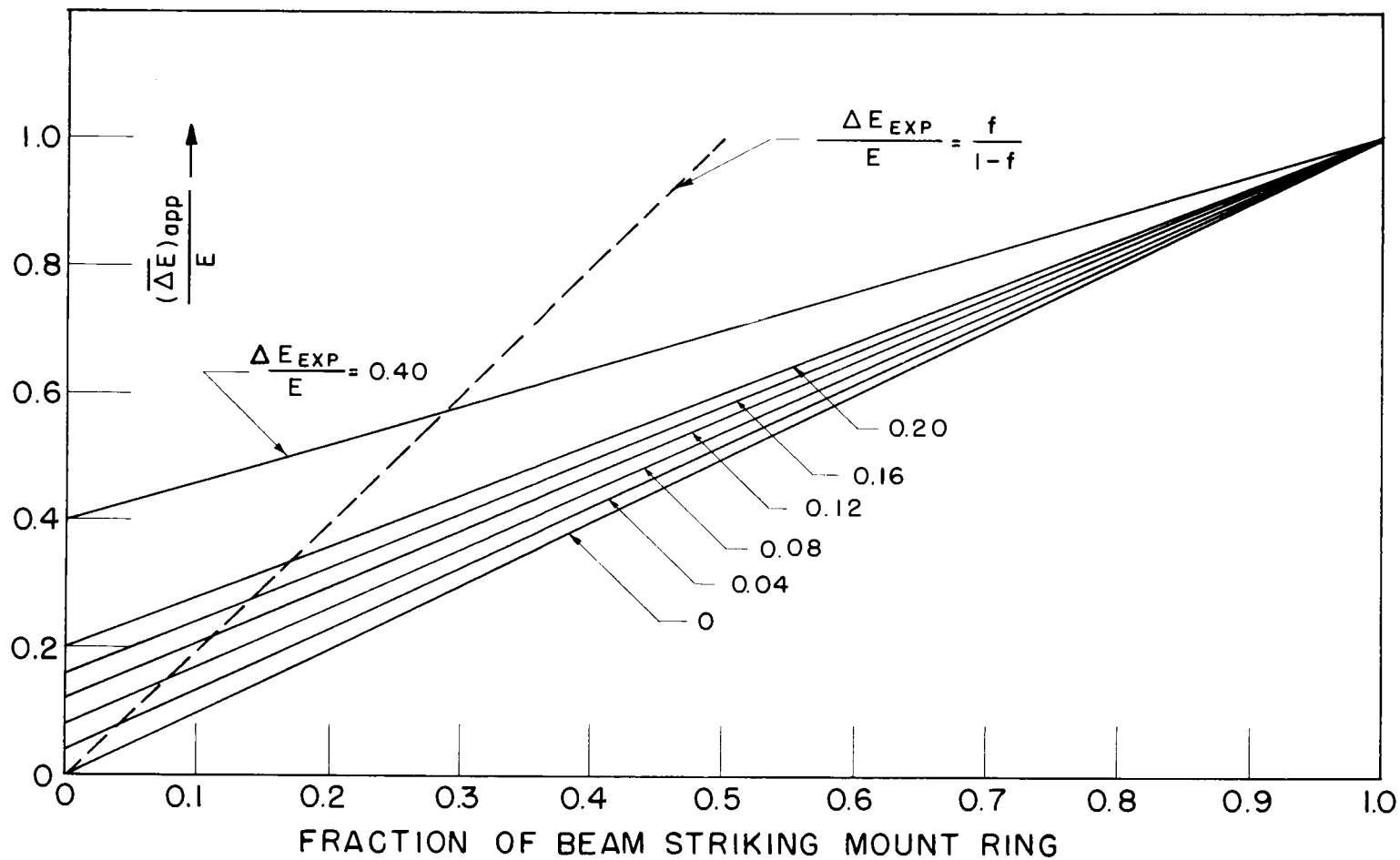

Fig. 5. Apparent Energy Loss as a Function of the Scattered Fraction of the Beam.

UNCLASSIFIED
ORNL-LR-DWG. 39719

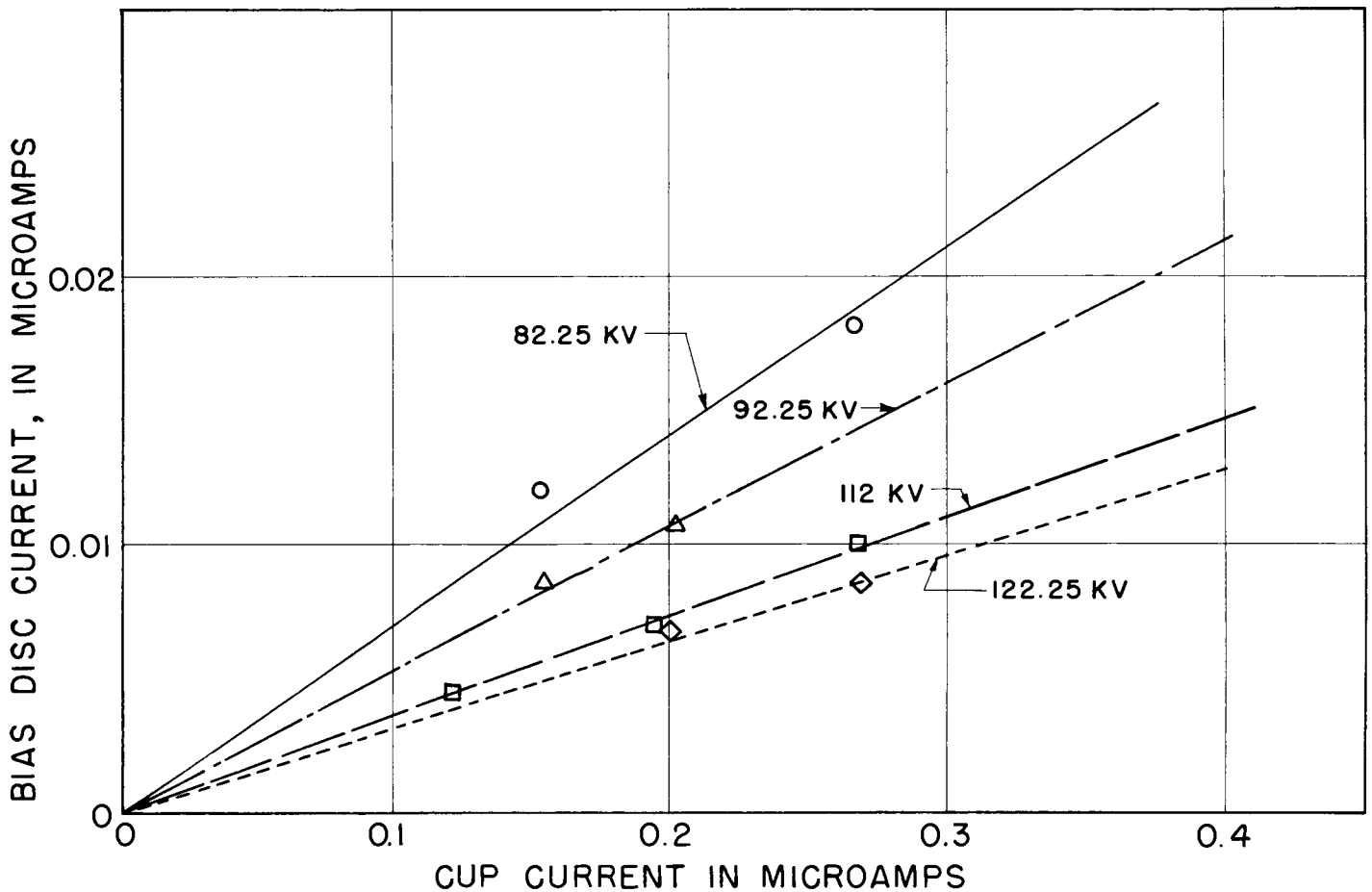

Fig. 6. Bias Disc Current Due to Scattering at Various Energies.

foil and the ring geometry of Case b, Figure (4), both of which increased the single scattering. These results seemed to further substantiate the assumption that there was definite scattering into the mounting ring and bias discs and that the fraction f was independent of the beam current.

2. Multiple Scattering and Increased Path Length

When the bombarding electron collides with a nucleus of an atom in the absorber, it is scattered essentially without energy transfer. In the case of multiple scattering, a number of these collisions take place before the electron emerges from the absorber, and the net effect is an increase in path length for the electron. Thus, in measuring stopping power, one should correct for this increase in the effective thickness of the absorbing medium in order to obtain the correct energy loss per unit path length. This correction is readily calculated using the multiple scattering theories of Williams[30] and Moliere[31].

The total increase in path length is given by Kalil, et. al.[32] to be

$$\overline{\Delta \ell} = \int_0^t d\ell = 1/2 \int_0^t \overline{\theta^2}\, dt \qquad (50)$$

where $\overline{\Delta \ell}$ is increase in path length, t is foil thickness and θ is scattering angle.

θ_2 is the mean square scattering angle and is given by

$$\overline{\theta^2} = t\, \frac{4\pi NZ(Z+1)\, e^4\, (1-\beta^2)}{m_o^2\, v^4} \ln \left[4\pi Z^{1/3}\, (Z+1)\, Nt(\hbar/m_o v)^2 \right] \qquad (51)$$

$$\equiv at \ln bt$$

---

[30] E. J. Williams, Proc. Roy. Coc. 169A, 531 (1939); Phys. Rev. 58, 292 (1940).

[31] G. Moliere, Z. Naturforsch 3a, 78 (1948).

[32] Kalil, F., et. al., op. cit.

where $N = N_A \rho / A$, Z, A = atomic number and atomic weight of foil material, e = electronic charge, $\beta = v/c$, and m_o = electron rest mass.

This value for θ^2 is based on Williams' Theory[33] of multiple scattering and its derivation is given in detail by Kalil, et. al. When Equation (51) is substituted in Equation (50), the increased path length $\overline{\Delta \ell}$ becomes:

$$\overline{\Delta \ell} = \frac{at^2}{4} \left[\ln (bt) - 0.5 \right] \tag{52}$$

where a and b are defined in Equation (51).

---

[33] E. J. Williams, op. cit.

III. APPARATUS

The apparatus used for measuring electron stopping power is described in detail by Kalil, et. al[34] Briefly, the instrument consisted of an electron gun (with power supply), an accelerating tube, a target foil, and a Faraday Cup (see Figure 7). A monoenergetic electron beam from the gun was accelerated down the tube, struck the foil with a known energy, and was collected in a Faraday cup immediately behind the foil. Energy imparted to the foil by the transmitted beam was measured calorimetrically. The electron gun will be discussed in some detail and the accelerator and the apparatus for measuring the energy imparted to the foil described in a general way.

A. Electron Gun and Power Supply

1. Electron Gun

Previous to this work, the electron gun used with the apparatus was a General Electric 3MP1 cathode ray tube. Guns of this type were purchased with the screen removed. Because these guns were the oxide cathode type, they had to undergo an activation process whenever exposed to air and before each use. This activation process proved to be unreliable, and tubes often had to be replaced after relatively short use. For this reason the gun was modified as shown in Figures (8) and (9). The electrode structure was that of a 3MP1 tube, but with the glass envelope, base, filament, and cathode removed. The remaining structure was inserted into a brass mounting which fitted into the existing gun mount on the accelerator. The leads to the grid, first anode, second anode, and deflection plates were spot-welded to

[34] Kalil, et. al., cit.

UNCLASSIFIED
ORNL-LR-DWG. 37738

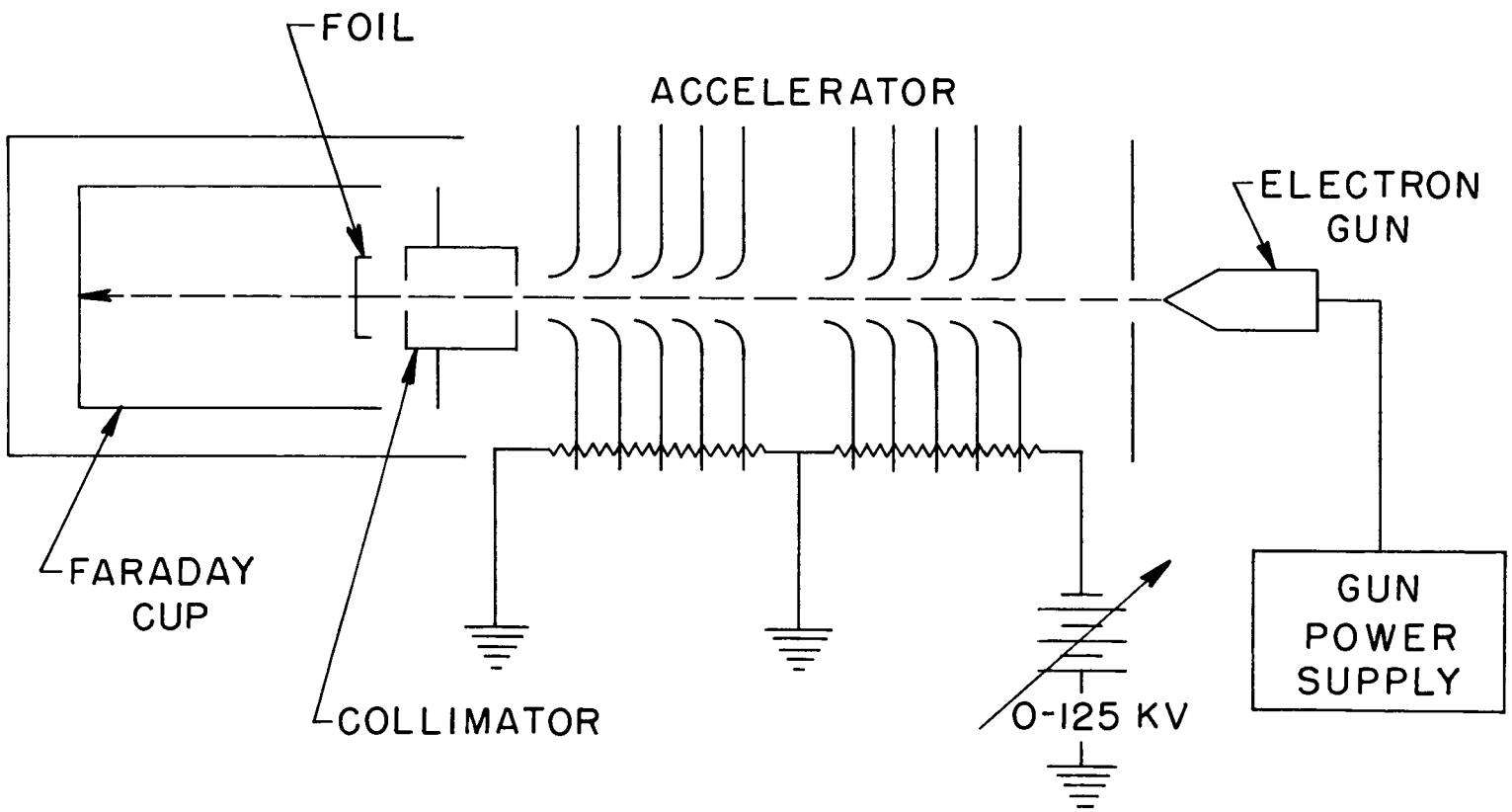

Fig. 7. Schematic Diagram of the Apparatus.

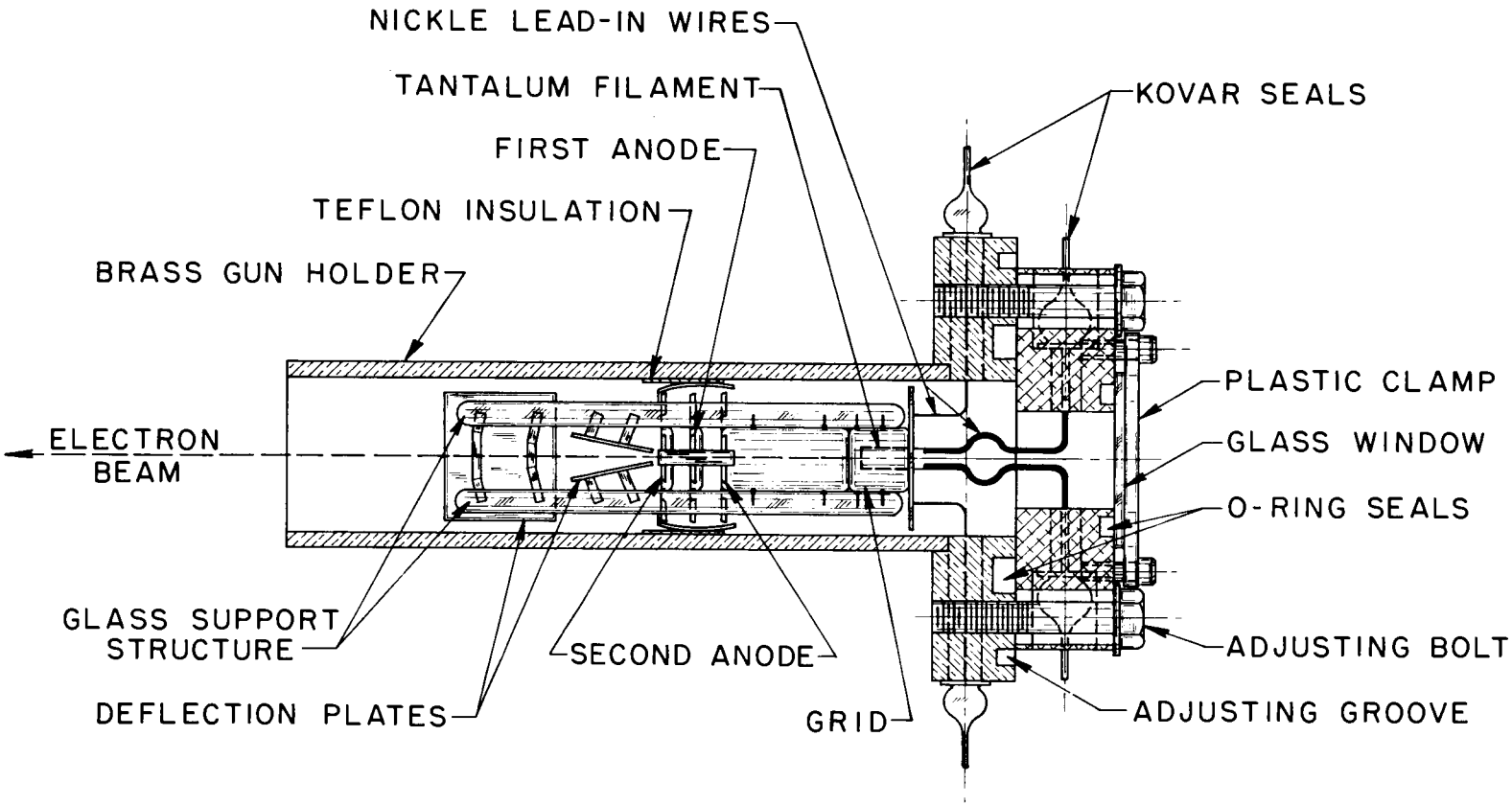

Fig. 8. Cross Section of Electron Gun and Mount.

UNCLASSIFIED
PHOTO 45950

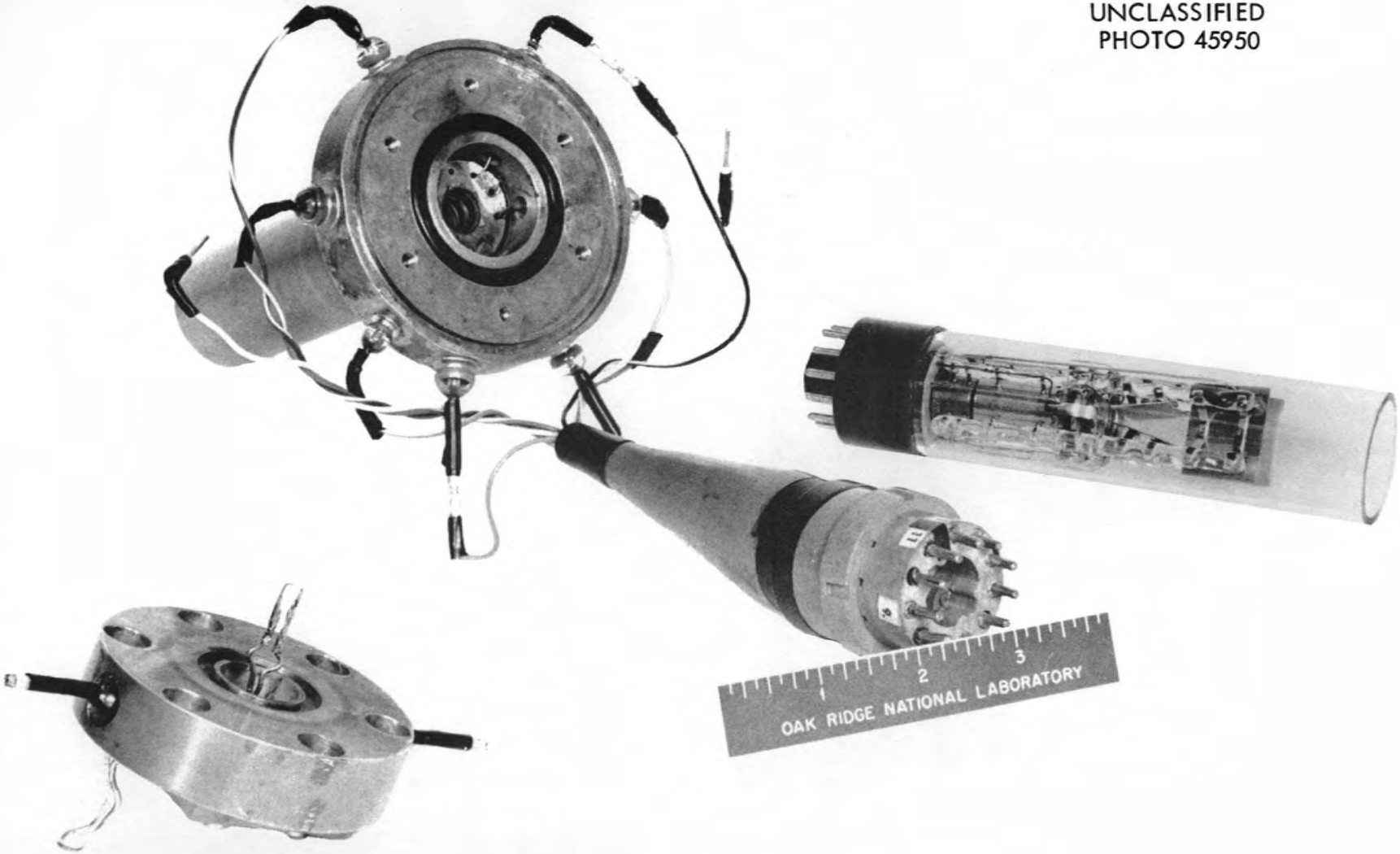

Fig. 9. The Electron Gun and Filament.

nickel lead in wires, which passed into the brass tube through kovar seals. The gun was completely insulated from the brass tube by a strip of teflon as indicated in the figure.

The second part of the gun was the plate which supported a special tantalum filament. This filament was cut from a sheet of tantalum weighing 50 milligram per square cm. to form a ribbon 1/16 inch wide and 1-1/4 inches long. The ribbon was then bent into a U shape, tapered slightly in the middle where the greatest heating was desired, and spot-welded to large (No. 20) nickel lead-in wires. Again the wires passed out through the plate through kovar seals. As shown in the schematic diagram of the gun, the filament was suspended by its nickel leads down inside the cup-shaped grid. For best results and control of the beam by the grid, it was important that the filament-to-grid distance be of the same magnitude as the grid-aperture radius[35] ($\sim$ 1/32 inch).

In order that the filament could be adjusted directly over the grid-aperture, the end plate was made with a window that allowed direct observation of the filament when the gun was assembled. This window was a 1-1/2 inch square glass plate clamped in place over an O-ring seal by a larger rectangular plastic clamp. The plastic gave strength to the window; the glass served to isolate the plastic from the vacuum, thus preventing the plastic from outgassing into the system when the filament was hot.

Positioning the filament in front of the grid aperture could be accomplished after the gun was completely assembled. When the adjusting bolts were loosened slightly, the filament mount could move in any direction laterally due to the large 7/16 inch holes through which the bolts passed.

---

35 K. R. Spangenberg, VACUUM TUBES, (McGraw-Hill Book Co., 1948) pp. 416-417.

A screwdriver or similar tool inserted in the adjusting groove facilitated movement of the filament mount.

Tantalum has a number of properties which make it desirable as a filament. It is almost completely immune to corrosion and chemical attack; it is strong and ductile; it has a high melting point, low-vapor pressure, and low thermal expansion; and it has good thermionic emission, its work function of 4.19 volts being just slightly lower than tungsten. It was found that a filament current of 4 to 5 amperes gave an excellent electron beam.

This electron gun gave unusually dependable service but it occasionally required replacement of the filament. It was a simple matter to remove the filament support and spot-weld a new tantalum ribbon to the nickel leads.

2. Power Supply

The power supply for the electron gun is shown schematically in Figure (10). Panel meters gave the voltages and currents of all the gun elements. The 125 KV power supply was connected to the second anode and to the plate of the accelerator. This meant that electrons always entered the accelerator with a kinetic energy equal to the second anode potential, for the gun cathode was then at second anode potential below the end plate.

Focusing and aiming the beam was accomplished by varying the potentials of the gun elements (deflection plates, first and second anode, and grid). The beam could be further aimed by varying the current through the vertical and horizontal magnetic de-gaussing coils. These have a separate power supply and carry DC currents up to 8 amps.

Two isolation transformers in cascade supplied the 110 AC line voltage to the gun power supply. All apparatus at high voltage, including the gun

UNCLASSIFIED
ORNL-LR-DWG. 37741

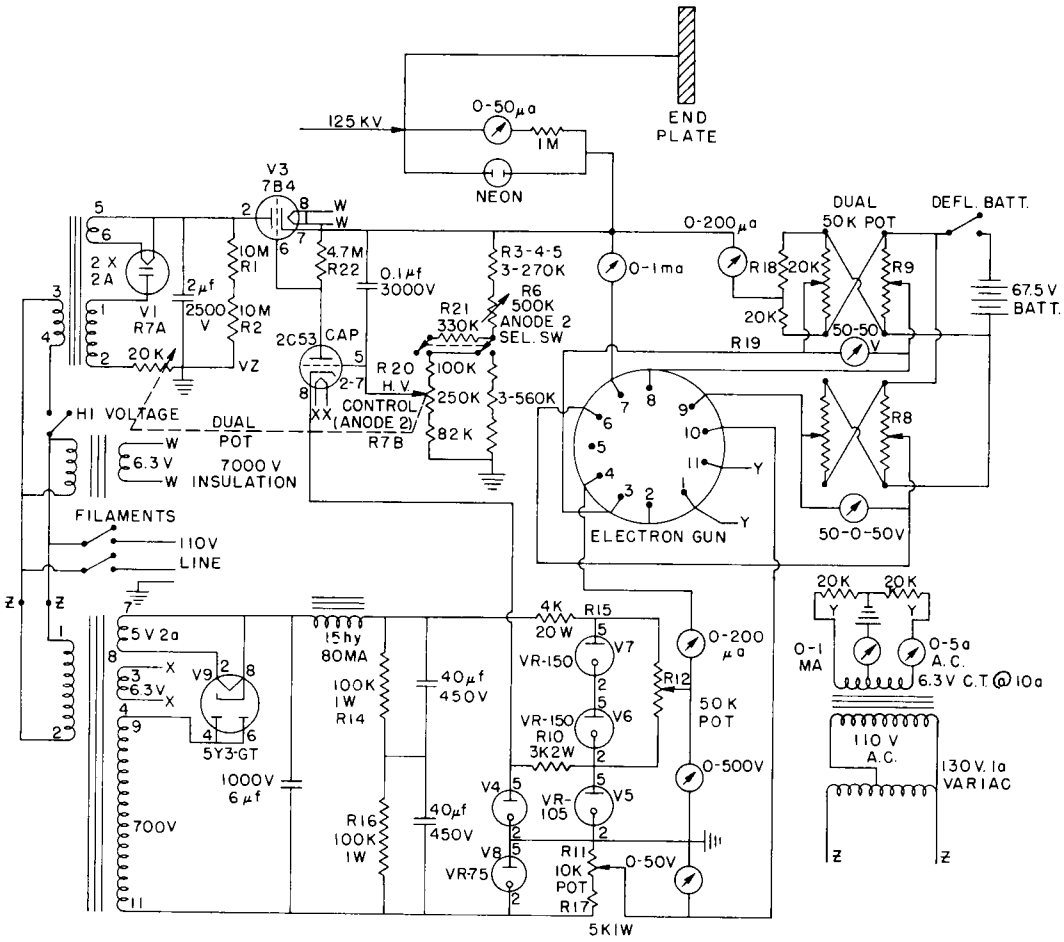

Fig. 10. Electron Gun Power Supply.

power supply and the accelerator, was enclosed in a screen "cage". The power supply controls could be operated from outside by using insulating rods attached to the controls.

B. Accelerator

The accelerating tube was of the Cockcroft-Walton type and consisted of alternate ceramic insulators and accelerating electrodes sealed vacuum tight. Six fifty-megohm IRC voltage dividing resistors in series established the electrode potentials. Note in Figure (7) that only the first half of the tube was used to accelerate the beam. The second half of the tube was grounded for this experiment.

High voltage for the accelerator was supplied by a center grounded Westinghouse 250 KV X-ray power supply.

To aid in aiming and collimating the electron beam, a combination aiming screen and collimator was located at the end of the accelerator. This unit had two circular apertures with geometry such that an electron that passed through both openings could strike the foil only. Plastic insulators isolated the unit electrically from the rest of the system, the only connection being to ground through a sensitive galvanometer (see Figure 11). A Rubicon galvanometer of sensitivity 0.00406 microamperes per millimeter read the current when the beam struck any portion of the gold-plated aluminum screen and collimator. Aiming was accomplished by varying the potentials of the electron gun deflection plates and by varying the current through the magnetic de-gaussing coils. The galvanometer current was a minimum when the beam passed through the aperture and was correctly aimed.

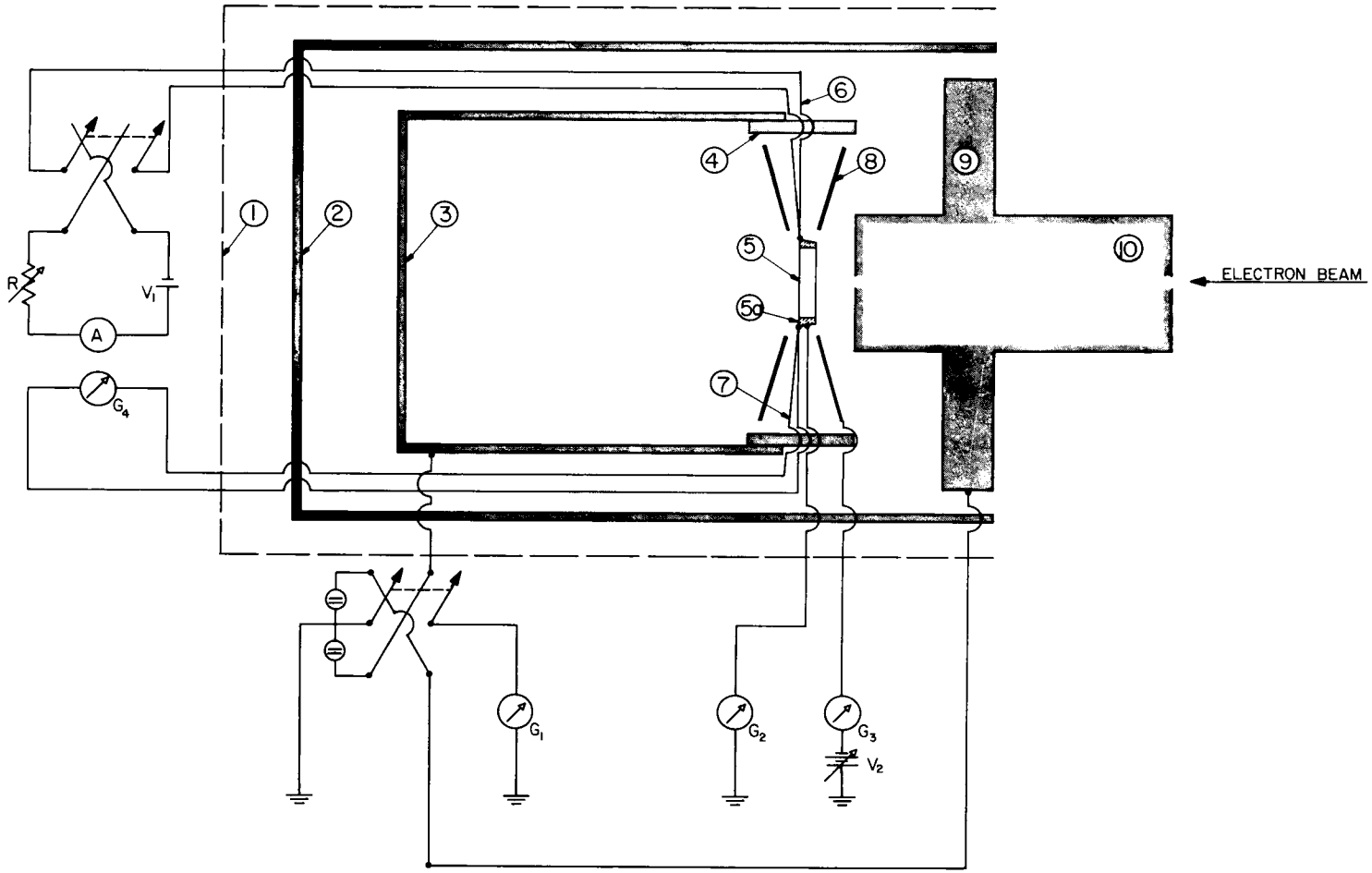

Fig. 11. Schematic Diagram of Apparatus for Measuring Beam Current and Foil Temperature.

Parts List For Schematic Diagram of Apparatus

1. Insulating Cylinder

2. Electrostatic Shield

3. Faraday Cup

4. Heat Sink

5. Foil

5a. Copper Mounting Ring

6. Cooling Thermopile

7. Temperature Monitoring Thermopile

8. Bias Discs

9. Aiming "Screen"

10. Collimator

G_1 Cup and Collimator Current Galvanometer

G_2 Foil Current Galvanometer

G_3 Bias Disc Current Galvanometer

G_4 Temperature Monitoring Galvanometer

V_1 1.5 Volt Cooling Battery

V_2 Variable Negative High Voltage

R Variable Cooling Resistance

C. Apparatus for Measuring Energy Loss

To measure stopping power calorimetrically, the amount of energy per unit time dissipated as heat in the foil by the transmitted beam was to be determined. Therefore, a means of keeping the environment of the foil at a constant temperature and a method of determining the temperature rise in the foil due to the electron beam were needed. It was also necessary to determine the beam current passing through the foil in order to relate the dissipated power to the energy lost. These quantities were determined with the equipment shown in Figure (12) and discussed below. It is described only briefly and the reader is referred to Kalil, et. al. for a detailed discussion.[36]

1. Temperature Control

The environment of the foil, including the Faraday cup, mounting parts, and all related pieces were completely enclosed in a heavy copper cylinder 12 inches in diameter. This cylinder was wrapped with 40 feet of heating wire and thus acted as a low temperature furnace. A thermostat controlled the power to the heater and held the temperature within 0.01 centigrade degrees of the desired temperature which was usually several degrees above room temperature.

Inside the heater cylinder was a concentric aluminum cylinder 6 inches in diameter which actually housed the foil, Faraday cup, collimator, and their related parts. This cylinder bolted directly to the end of the accelerator and was wrapped with a thick layer of asbestos tape to further insulate its contents from the small cyclic temperature changes of the heater. Between the aluminum cylinder and the copper heater was an air

---

[36] Kalil, et. al., op. cit.

UNCLASSIFIED
PHOTO 45947

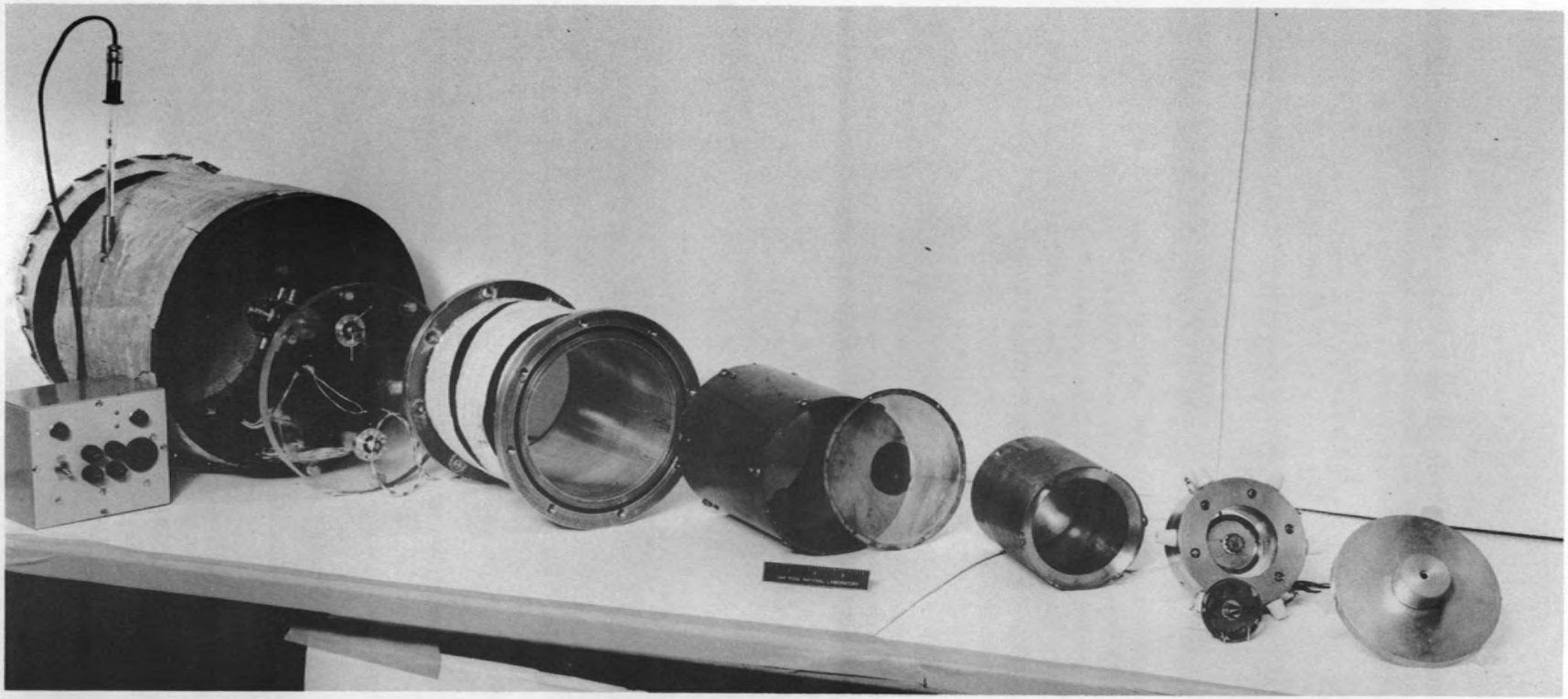

Fig. 12. Disassembled View of Apparatus for Measuring Beam Current and Foil Temperature.

space which further insulated the system.

2. Apparatus for Measuring Temperature Rise in the Foil

The mono-energetic electron beam, after being accelerated down the tube, passed through the two collimating slits, struck the foil, and delivered energy to the foil as heat, thus causing a temperature rise in the foil proportional to the beam energy absorbed. This temperature change was measured by a thermopile consisting of a set of six copper-constantan thermocouples placed around the periphery of the foil. The thermal EMF of this thermopile was measured by a Leeds and Northrup galvanometer whose sensitivity was 0.050 microvolts per millimeter deflection.

A second set of thermocouples indentical to the temperature monitoring pile was added to the system to cool the foil by the Peltier effect. A complete discussion of the methods of measuring the power dissipated using these thermopiles is given in Chapter V.

The copper-constantan thermocouples served an additional purpose in that they supported the foil and foil holder as can be seen in Figure (13). It was necessary, then, in choosing thermocuoples, to select couples that would have relatively high EMF's, be mechanically strong, and yet be small enough to keep conduction heat losses to a minimum. Number 40 gauge copper and number 38 constantan were chosen for this purpose. The hot junctions of all couples were embedded uniformly around a special plastic ring which held the foil holder and foil. This provided good thermal contact between the foil and the hot junctions and at the same time kept them electrically insulated from each other. The reference junctions for the thermocouples were at the heat sink which remained at constant temperature due to its

UNCLASSIFIED
PHOTO 45953

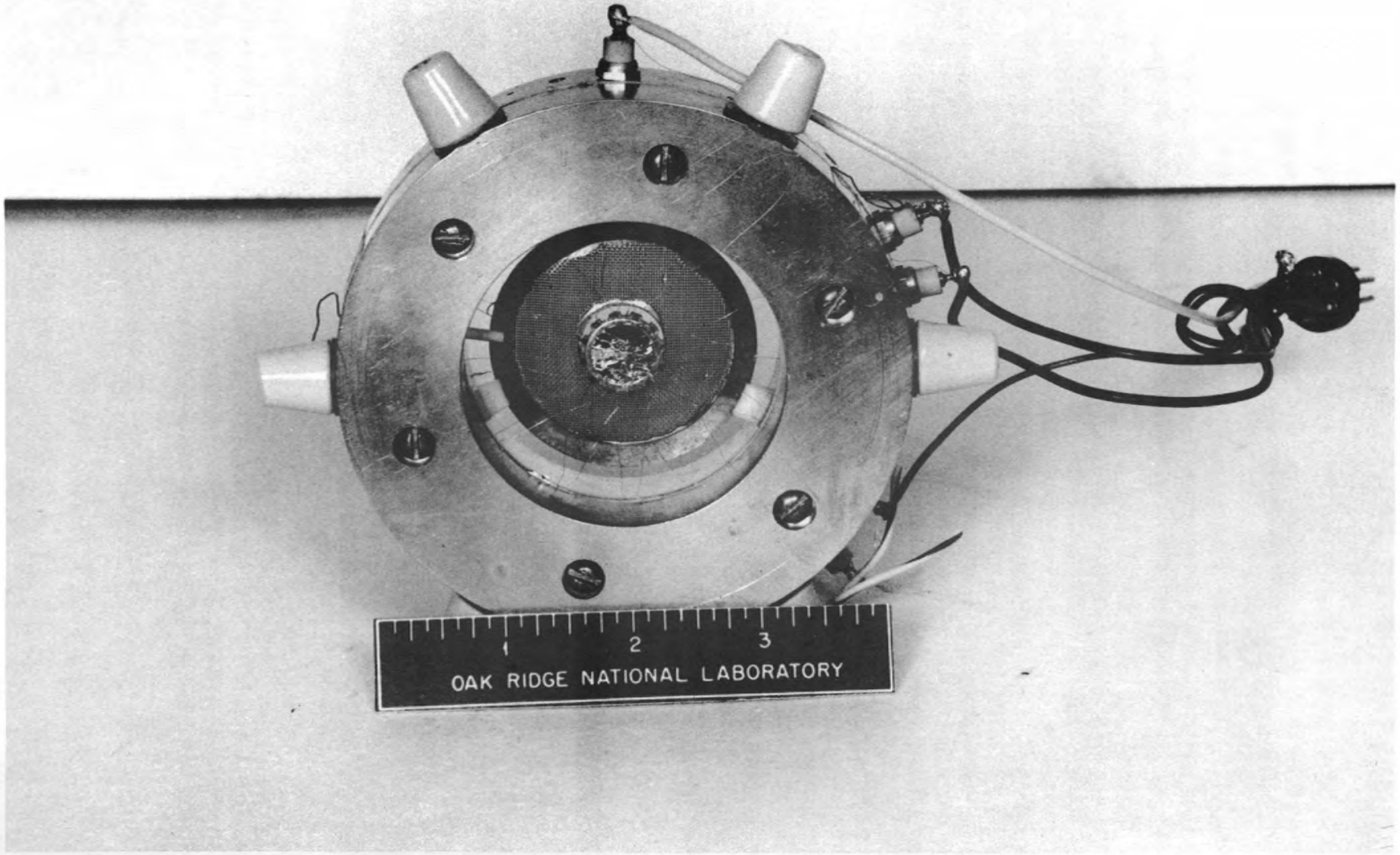

Fig. 13. Heat Sink and Foil Mount with Foil in Place in Center.

large mass and the temperature control.

The hot junctions were made by welding the copper and constantan wires in a mercury bath under a helium atmosphere using AC current. This method, described in detail elsewhere[37], gives mechanically strong junctions.

The reference junctions were formed by crossing the thermocouple wires and pressing them together between the two halves of the heat sink. That is, each junction was formed by sandwiching an appropriate copper and constantan wire between thin copper wedges and clamping all such junctions between the halves of the heat sink. These junctions were electrically insulated from the heat sink by thin teflon rings which completely covered the inner faces of the heat sink sections. Figure (14) shows the wiring for one thermopile (six couples).

As shown in Figure (11), the galvanometer G_4 monitored the foil temperature being connected directly across the temperature monitoring thermopile. This galvanometer was a Leeds and Northrup external scale type with sensitivity of 0.05 micro-volts per millimeter, critical damping resistance of 8 ohms, internal resistance of 14.3 ohms, period of 6.2 seconds and a focal length of 1 meter.

Because of its sensitivity, and because the thermal EMF's produced at the thermocouple junctions were of the order of 5 microvolts, it was necessary to reduce any extraneous EMF's which might arise from junctions outside the system. Although the room was air-conditioned and maintained at about a constant temperature, slight fluctuations in temperature could give rise to extraneous EMF's at junctions. To minimize this effect continuous teflon covered copper wires led from the galvanometer to the thermopile. These were twisted together along their full length of 15

---

[37] Kalil, et. al., op. cit.

UNCLASSIFIED
ORNL-LR-DWG. 37740

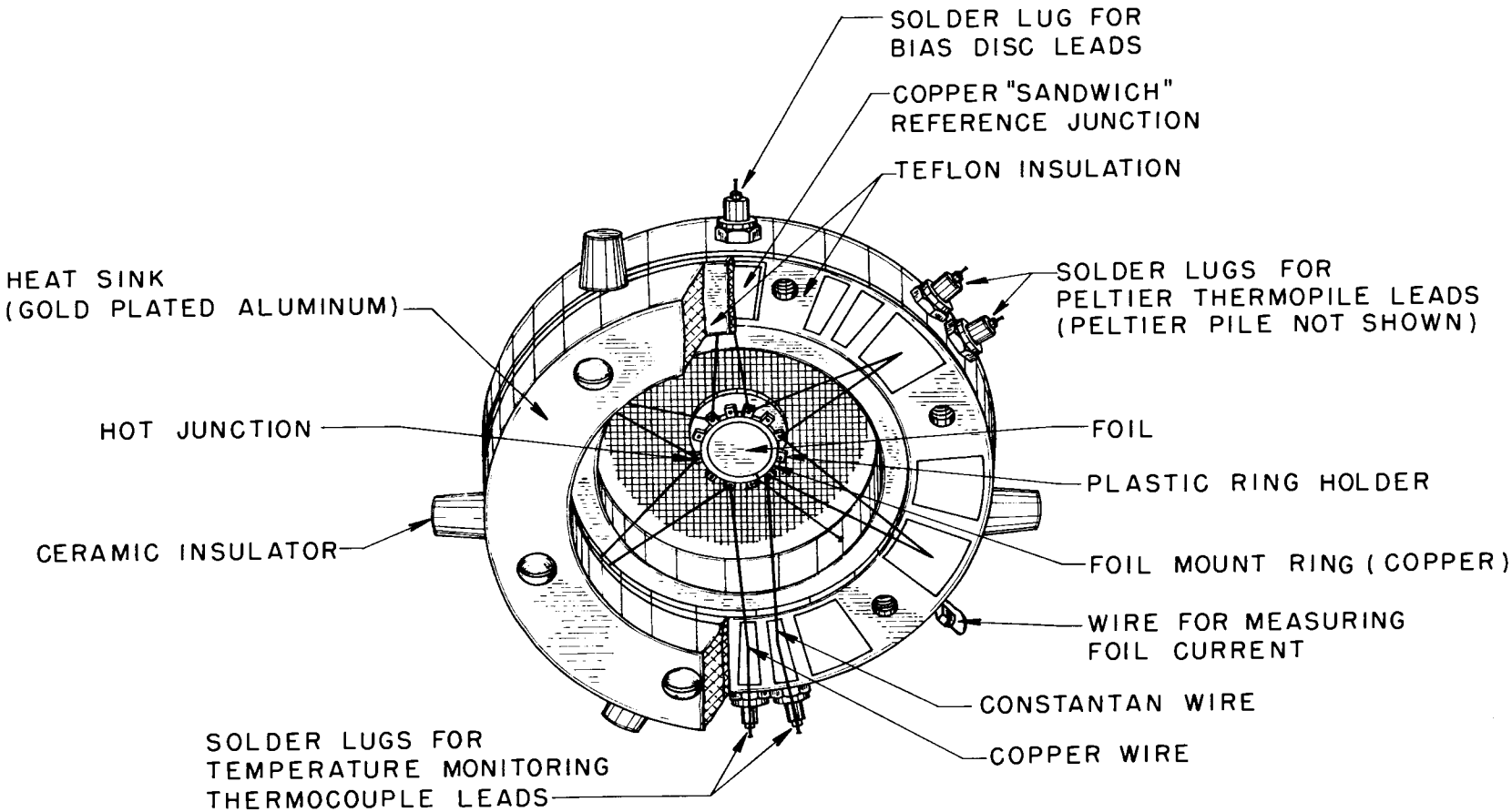

Fig. 14. Cutaway of Heat Sink and Foil Mount Showing Wiring for One Thermopile.

feet to eliminate AC pick up. The only junctions involved were at the thermopile and at the galvanometer. Since the thermopile was inside the system and maintained at a constant temperature there was no problem of extraneous EMF's at this point. There remained, then, only the galvanometer junctions to consider. To keep those junctions at a constant temperature, a special insulating housing to enclose the galvanometer was built of foam plastic. This insured that changes of temperature were small in the environment of the galvanometer. A glass window in the housing allowed the galvanometer mirror to be used in the usual manner.

A special vibration free mount for the galvanometer consisted of a heavy steel rectangular base set in a sand-filled box.

Using these modifications, the temperature monitoring galvanometer kept its zero very well. Drift over a period of a day was never more than 3 cm from the original zero. Throughout a run the change in zero was usually negligible.

3. Apparatus for Measuring Beam Current

A faraday cup was located immediately to the rear of the foil and collected the transmitted beam from the foil. This cup had 3/8 inch thick brass walls and a 3/4 inch aluminum end plate. It served to absorb any X-rays produced, thus eliminating secondary electrons at its external surface. The cup was connected to ground through a galvanometer, G_1, (see Figure 11), of sensitivity 0.00406 microamperes per millimeter. A grounded electrostatic shield around the cup reduced extraneous currents due to pickup. This shield was a 5-7/8 inch diameter cylinder of $\frac{1}{4}$ inch aluminum copper plated. The end plates of the shield were of brass screen mesh to aid in evacuating

the air from the system during pump-down.

Two wire mesh bias discs mounted on teflon insulators were located on each side of the foil. These discs carried a large negative voltage supplied by an Atomics Instrument Company, Super Stable, high-voltage power supply with a negative voltage output. This negative voltage helped maintain accurate beam current measurements by repelling secondaries from the Faraday cup back into the cup. In addition, any secondaries leaving the foil were repelled back into the foil so that they could dissipate their energy there in keeping with definition of stopping power. A Leeds and Northrup galvanometer, G_3 (see Figure 10), of sensitivity 0.000424 microamperes per millimeter, was connected in series with the bias discs and the negative high voltage and read the current due to any high energy primaries which emerged from the foil at wide enough angles to strike the discs. Thus, the true beam current consisted of both cup and bias disc current although the latter was always much smaller than the former.

In addition, the foil was connected through a galvanometer to ground so that any primary beam electrons stopped completely in the foil would give a foil current. One would expect to find foil currents only at low calibrating voltages when the beam was completely stopped in the foil.

Electrical connections for all the above mentioned components passed out of the system through the plastic end plate by means of a brass tube with Kovar seals and Amphenol connectors.

Although i_B, the beam current, was the sum of i_{cup}, i_{Foil}, and i_{bias}, the foil and bias currents were zero throughout the copper runs so that $i_B = i_{cup}$. The bias disc voltage was kept at a high negative voltage in

the range of -1000 volts so that essentially all secondary electrons were turned back to the foil.

The effect of the bias discs voltage in repelling secondaries is shown in Figure (15). For this curve, a beam of low energy electrons was used in order to give more scattering and hence a more detectable bias disc current.

4. Auxiliary Equipment

The accelerator was evacuated using three pumps: a small Welch Scientific company Duo-Seal vacuum pump used in roughing down, a large Welch Duo-Seal vacuum pump, and a type VMF-260-R Distillation Products Industries oil diffusion pump. The large Duo-Seal pump and the diffusion pump were run continuously and could be sealed from the system by an isolation valve when the accelerator was open to air. To evacuate the accelerator, the small pump was used to bring the pressure down to the order of 100 microns of mercury as read on a Hastings Model GV-3 Vacuum gauge. The system was then opened to the large Duo-Seal and the diffusion pumps, lowering the pressure to 10^{-6} millimeters of mercury as read on a Consolidated Electrodynamics Corporation Type VG-1A ionization gauge.

To protect the water-cooled diffusion pump in the case of a water line failure, a water interlock was added which would turn the diffusion pump heater off automatically in the event the water supply to the building was cut off. A single pole, single throw Mercoid Switch made by the Mercoid Corporation of Chicago was used for this purpose. It was connected directly to the water line, and was set to break the circuit when the water pressure fell below 24 pounds.

In order to determine the rate of temperature rise in the foil, it was

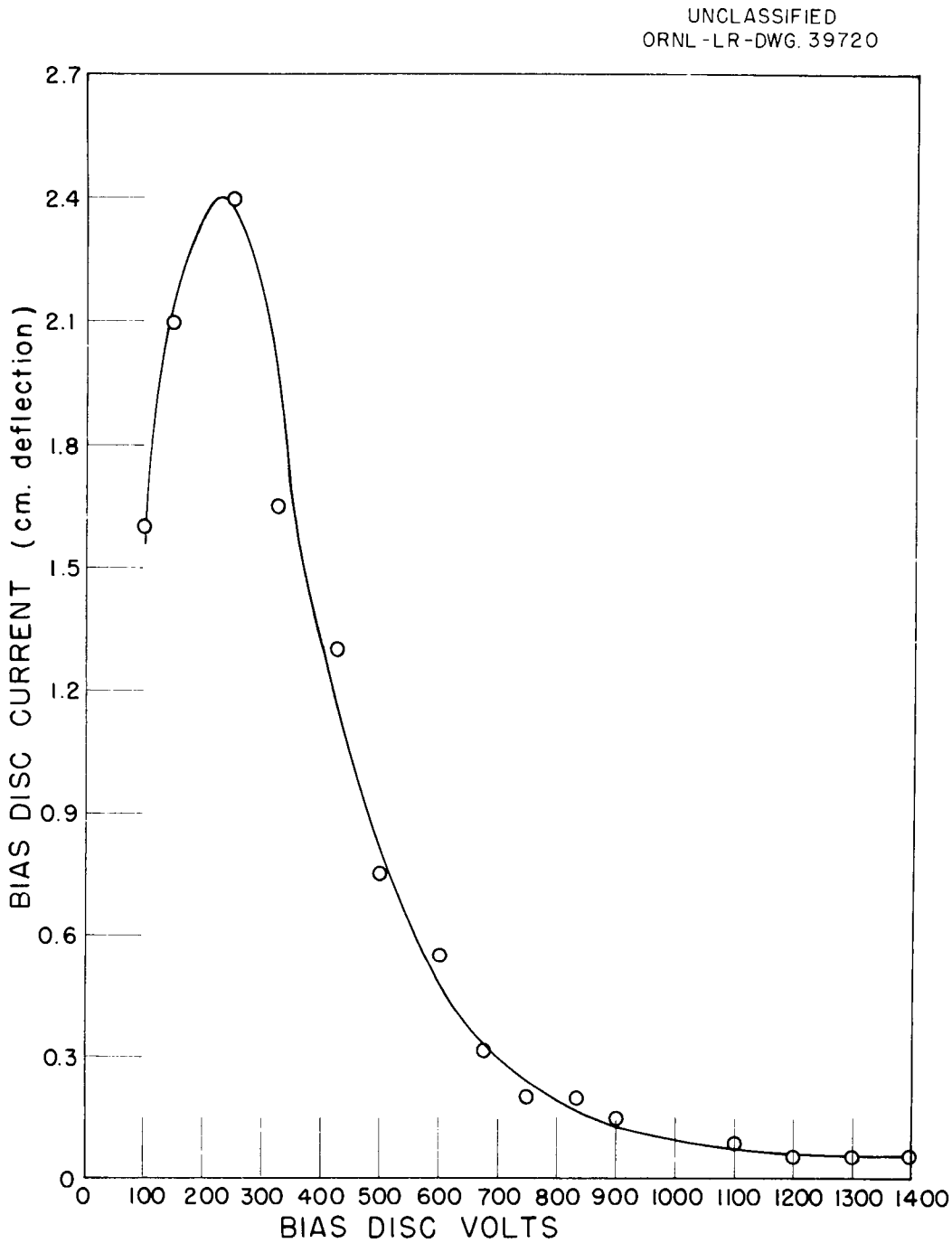

Fig. 15. Bias Disc Current as a Function of Bias Voltage.

necessary to read the temperature monitoring galvanometer at convenient time intervals. A synchronous motor which turned 10 revolutions per minute when operated from the 60 cycle AC line voltage was used to trigger a buzzer once each revolution, so that a signal sounded every 0.1 minutes. Galvanometer readings were recorded manually at these intervals.

The cooling circuit consisted of a 1.5 volt No. 6 dry cell in series with an ammeter, a reversing switch and a variable resistance as shown in Figure (11). The switch allowed the thermopile to be used either for cooling or for heating the foil. The variable resistance was a ten turn 1000 ohm helipot which allowed the current through the pile to be varied from 0-10 milliamperes. The ammeter was a Weston, Model 45 voltmeter with a Weston external shunt. This instrument, when connected to the shunt, read International Amperes and was calibrated correct to 1/4 of one per cent of full scale at any part of the scale.

IV. TECHNIQUES FOR MAKING FOILS

A number of methods for producing thin metallic foils are described in the literature [38]. Several additional methods were devised for this work to meet the problems which arise in the production and handling of foils of the order of 100 micrograms per square centimeter in thickness.

The general method used for foil production was vacuum evaporation of the metal onto the surface of a glass plate. Assuming isotropic evaporation, the foil thickness depends on the inverse square law

$$t = \frac{mh}{4\pi r^3} \tag{53}$$

where t is the foil thickness in grams per square centimeter, m is the mass in grams, h is the perpendicular distance between the source and the plance of the foil, and r is the distance from the source to any point on the foil.

A. The Vacuum Evaporator

The vacuum evaporation system was designed especially for producing thin foils. The main parts of the apparatus were the pumping system, the evaporation chamber, and the electrical services.

1. Pumping system

A Consolidated Electrodynamics Corporation type MCF oil diffusion pump was connected to the evaporation chamber through a

[38] See for instance L. Holland, VACUUM DEPOSITION OF THIN FILMS, (Chapman and Hall, Ltd. London. 1956.)

liquid nitrogen cold trap. This pump used special silicone oils to minimize oxidation of pump oil by air entering the pump. A gate type isolation valve allowed the diffusion pump to be kept under vacuum and at operating temperature at all times, even when the evaporation chamber was open to the atmosphere.

The evaporation chamber was roughed down by means of a Duo-Seal mechanical fore-pump. This pump also acted as a backing pump, for it could be connected first to the chamber and then to the backing side of the diffusion pump.

A Hastings Model GV-3 vacuum gauge was used to read pressures above 10 microns in the chamber. Pressures down to 10^{-7} millimeters of mercury were read with a General Electric ion gauge using a Consolidated Electrodynamics Corporation Type VG-1A ionization gauge.

The diffusion pump was protected by a Mercoid Switch which cut the pump heater off in case of water failure in the cooling line. This switch, made by the Mercoid Company of Chicago, was a single pole, single throw, mercury-contact switch set to break electrical contact when the water pressure fell below four pounds of pressure.

A large five inch diameter neoprene exhaust hose was added to the exhaust outlet of the fore-pump so that the system could be used for evaporating such toxic metals as beryllium. An exhaust fan at the roof of the building kept the hose under negative pressure at all times.

2. Evaporation Chamber and Electrical Services

The evaporation chamber was a typical bell-jar chamber. A steel-mesh cylindrical shield was used to cover the bell-jar for safety purposes

The chamber, with jar removed, is shown in Figure (16). The components used for the evaporations included four electrodes, a rotary shutter, and a support stand for the glass plates. The electrodes served as mechanical supports for and electrical leads to the filaments. A series of switches external to the chamber allowed heating of any desired filaments by currents up to 200 amperes. The rotary shutter could be rotated by an external control to a position directly over the filaments, thus shielding the glass plates from undesirable evaporation products. The support stand suspended the glass slides at the desired position above the filaments. Source-to-plate distances could be varied by adjusting the bolt adjustments of the electrodes, the support stand, or both.

B. Techniques of Foil Preparation

1. Preparation of Glass Slides

It is important in preparing thin foils that one have a smooth, clean surface on which to evaporate the metal. Glass micro-slides met this requirement, and proved to be entirely satisfactory for the purpose. The glass slides used were 25mm × 75mm × 1mm non-corrosive, non-fogging micro-slides manufactured by Clay

Fig. 16. The Vacuum Evaporation Chamber Showing Glass Slides on Support Stand and Electrodes.

Adams, Incorporated, of New York. These slides were wiped clean of dust or spots with lens paper such as Dow-Corning's silicone treated "Sight Savers". The glass slides were suspended 8 to 10 cm above the source as shown in Figure (16).

In the vacuum evaporation of metallic foils onto the surface of glass plates, difficulties were encountered in the subsequent removal of the foils from the plates. Thus, it was found desirable to coat the glass with some suitable backing material prior to the evaporation of the metal.

One technique that worked very well was to coat the glass with a water soluble material. The metallic foil was then evaporated over the backing material. Removal of the foil from the slide was accomplished by "floating" it off in water as illustrated in Figure (17). The water dissolved the backing layer between the foil and the glass plate, thus separating the two. The foil then floated on the surface of the water and was ready for mounting.

To assure a smooth even layer of backing material, the same evaporation techniques (as for the foil itself) were used.

In choosing a backing material, the following qualities were considered essential:

(1) The material must be water soluble.

(2) It should have a reasonable low melting point.

(3) It must evaporate and coat the glass slides smoothly.

(4) It must not react with the metal which it is backing.

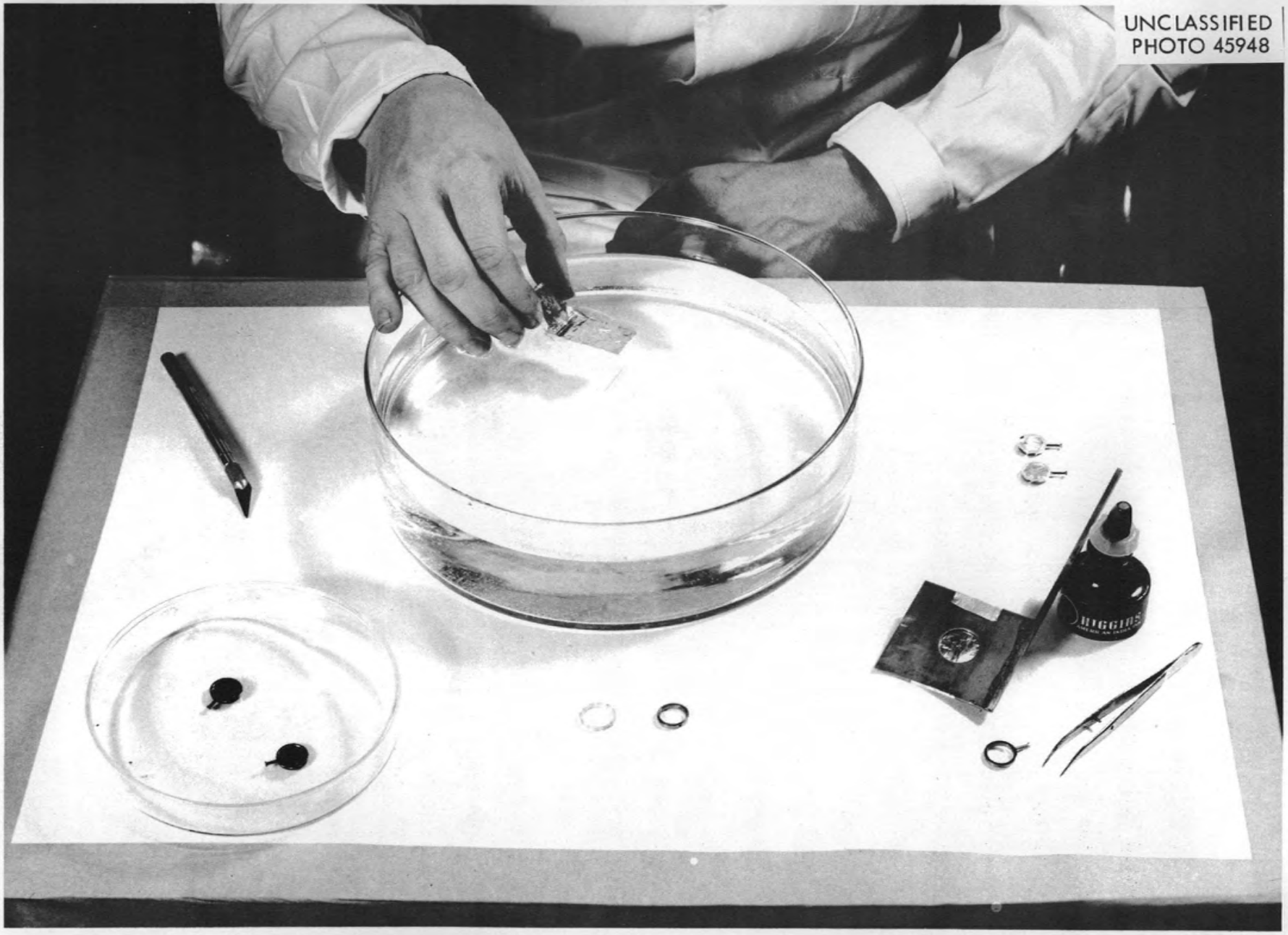

Fig. 17. Technique for Removal of Foil from Glass Slide.

The first two requirements allowed much flexibility in the choice of a material. The latter two, however, had considerable effect on the quality of foil, and care had to be taken to choose materials that met these requiremtnts.

One material that worked well as a backing material was "Victawet", an organic wetting agent manufactured by the Vicks Company. A technique using "Victawet" as a backing material was developed by J. Cathcart of the ORNL Metallurgy division and is described in detail by Kalil, et. al.[39]

Techniques using other materials were recently developed for this particular work using a number of inorganic compounds including AuCl, $Ni(NO_3)_2 \cdot 6H_2O$, $FeCl_3 \cdot 6H_2O$, $CaCl_2$, NaCl, and KF. These compounds were chosen on the basis of their properties as listed in standard chemistry reference handbooks. Of the materials used, KF generally gave the best results. The location of potassium high in the electromotive series of elements assures that it will not react with the evaporated metal foils during removal of the foil in water. In all cases, the backing materials were most successfully evaporated from tantalum "boat" filaments. Table I summarizes the properties of the various backing materials, the metals with which they were used, and the corresponding results.

2. Filaments

A large number of metals can be evaporated from refractory

---

[39] Kalil, et. al, op. cit.

TABLE I

BACKING MATERIALS

Compound	Melting Point	Boiling Point	Solubility		Type of Filament	State of Compound When Placed on Filament	Type of Foil	Results
			Cold Water	Hot Water				
Victawet	~ 400° C	~600° C	very soluble	very soluble	Tungsten -conical basket -Helix Tanatalum -boat	"Jelly"	Be Al Cu Ag Au	Bad - foils brittle Good Bad - foils brittle Good Fair
AuCl	170° C (d. to $AuCl_3$)	289.5° C (d.)	decom-poses	decom-poses	Tantalum -boat	Water solution	Au	Fair - foils not removed easily
$Ni(NO_3)_2 \cdot 6H_2O$	56.7° C	136.7° C	238.5 $\frac{g}{100ml}$	infinitely soluble	Tantalum -boat	Alcohol or water solution	Be Au	Bad - Be reacts with Ni Good
$FeCl_3 \cdot 6H_2O$	37° C	280° C	91.9 $\frac{g}{100ml}$	infinitely soluble	Tantalum -boat	Dissolve in alcohol, or acetone (alcohol best; gives even coating; no splattering during evaporation)	Be Cu Ag Au	Bad - Be reacts with Fe Good Good Good

TABLE I

(continued)

BACKING MATERIALS

Compound	Melting Point	Boiling Point	Solubility		Type of Filament	(Crystal, solution, etc)	Type of Foil	Results
			Cold Water	Hot Water				
$CaCl_2$	772°C	1600°C	59.5 $\frac{g}{100ml}$	159 $\frac{gm}{100ml}$ (at 1000°C)	Tantalum -boat	Crystals	Be	Fair - backing coat not smooth enough
NaCl	801°C	1413°C	35.7 $\frac{gm}{100ml}$	39.12 $\frac{gm}{100ml}$	Tantalum -boat	Crystals	Be	Fair - backing not smooth enough
KF	880°C	1500°C	92.3 $\frac{gm}{100ml}$	very soluble	Tantalum -boat	Crystals	Be Al	Good Good

metal sources such as tungsten, tantalum, and molybdenium bent to suitable shapes and forms. Two main types of sources were used: (1) Those made from wire bent in the form of conical baskets, helices or other suitable shapes, and (2) those made from metallic foil in the form of troughs, cylinders, or boats. In the first case, evaporation of the metal tended to be in all directions or into a 4π solid angle, while in the second, evaporation was restricted to a solid angle of no greater than 2π.

Choice of a filament depended upon the material to be evaporated. Many metals such as gold evaporated readily by wetting and flowing over the surface of a support. Others such as copper did not wet readily, while others alloyed with the filament instead. Thus, one had to choose a filament to meet the following conditions: (1) The metal should adhere to the filament; (2) the filament must have a vapor pressure such that it will not evaporate at a temperature below the melting point of the metal; and (3) the filament must not form an alloy which has a melting point below the evaporation temperature of the metal.

Generally, metals which did not wet a given filament readily could be evaporated easily from basket or boat type filaments so that the molten metal was well supported. Many useful suggestions given by L. Holland [40] were followed in this regard. Table II shows the methods used in evaporating various metals.

---

[40] L. Holland, op. cit. pp. 104-140.

TABLE II

FILAMENT AND FOIL VAPOR SOURCES

METAL	MELTING POINT	EVAPORATION TEMPERATURE (APPROXIMATE)	TYPE OF FILAMENT	REMARKS
Aluminum	660°C	1000°C	Tungsten -Multi-Strand Braid -Helical Coil -Sinusoidal Filament	-Wets at evaporation temperatures. -Alloys at higher temperatures.
Beryllium	1284°C	1250°C	Tungsten -Conical Basket -Boat Tantalum-Boat Carbon-Boat Zirconium-Boat Molybdenum-Boat	-Should wet Ta, W, and Mo. However, oxide film on surface impedes evaporation, so that much higher temperatures are needed. -Heavy Ta boats give best results. -Zr appears to alloy with Be well below evaporation temperature.
Copper	1083°C	1275°C	Ta Boat	-Does not wet readily.
Gold	1063°C	1465°C	Tungsten -Multi-Strand Braid	-Wets tungsten readily.
Silver	961°C	1050°C	Tungsten -Multi-Strand Braid -Conical Basket Tantalum-Boat	-Does not wet tungsten or tantalum. -Tight braid or coil will support for evaporation.

3. Evaporation Proceudres

The step by step procedure for preparing foils was as follows. First, filaments were prepared and bolted in place between the electrodes of the evaporation chamber. Next, an ample portion of backing material was placed in one filament, and a mass of the metal for the foil in another. The mass of metal used depended on the desired foil thickness as calculated from the inverse square law. The clean glass micro-slides were then placed in position on the support stand, and the rotary shutter was positioned between the filaments and slides. After the filaments and slides were in place, the bell-jar and its shield were replaced. The system was then evacuated using the fore-pump to "rough" the pressure down to 100 microns after which the diffusion pump was cut in.

After the vacuum was reduced to the order of 10^{-5} millimeters of mercury, current was sent through the filament containing the wetting agent. The filament was slowly heated until its contents melted. At this point, the shutter was rotated from between filament and glass plates allowing the evaporating backing material to coat the plates. The shutter was then returned to position over the filaments.

Evaporation of the backing material caused the pressure in the chamber to rise to about 10^{-4} millimeters of mercury. Hence, after evaporation of the backing material, the system was allowed to pump down before evaporation of the metal began.

In the filament holding the metal, the current was slowly increased to the point where the metal melted and flowed freely. At this point the shutter was again removed and the current increased greatly to give rapid evaporation of the metal. Normally only a second or two was required to coat the plates at which point the shutter was quickly rotated back into position and the current cut off.

To open the chamber and remove the plates, it was necessary only to close the gate-valve to isolate the diffusion pump and open the inlet valve. To minimize oxidation of the foils by air, and to aid in later pump down of the chamber, an inert gas (helium) was introduced through the inlet valve rather than air.

After removing the plates from the system, the foils were removed from the plates and mounted as described in the next section.

4. Removal of Foil from Glass Slide and Mounting of Foil

The foils were easily removed from the glass slides by slowly inserting the slide in a distilled water bath as shown in Figure (17). As the slide entered the water, the backing material dissolved and the foil floated on the surface due to surface tension.

To mount the foil on the copper support ring, the foil was first removed from the water using a rectangular flat metal "flag" with a circular aperture. This tool was inserted in the water and drawn out perpendicular to the surface so as to catch the foil and

stretch it across the aperture. Mounting on the ring was then accomplished by placing the "flag" over the ring concentric with the aperture. Excess foil around the ring was trimmed with a sharp instrument. It was found to be advantageous to coat the surface of the copper ring with India ink before mounting the foil. The ink acted as an adhesive and as a good electrical contact between foil and ring.

C. Weighing the Foils

1. The Modified Electrobalance

Foil thicknesses, in terms of micro-grams per square centimeter, were determined by weighing foils of known area. A modified Cahn Electrobalance, Model M10, was used for this purpose. The Cahn Electrobalance was originally intended for weighing samples in the range of 0 to 10 milligrams. By suitable modifications, however, it can be used in the 0 to 0.1 milligram (100 micro-gram) range. The modifications used were incorporated originally by Kalil, et. al.[41] and are described in detail by them. These modifications served to increase the precision of the instrument by reducing the absolute standard error from about 5 micrograms to 0.1 micrograms.

The electrobalance operates on the principle of balancing the torque due to the sample hung from an arm by an electromagnetic torque proportional to an electric current which can be measured

[41] Kalil, et. al., op. cit.

accurately. The circuit of the modified balance is shown in Figure (18).

Weighings were made by varying the current through the torque motor to balance the torque due to the sample. The potential drop across a precision resistance in series with the motor was directly proportional to the current and could be measured accurately with a potentiometer. The original internal potentiometer circuit and null detector of the electrobalance were replaced by a Leeds and Northrup, type K-3, potentiometer and a General Electric galvanometer with sensitivity of 0.016 microamperes per millimeter.

A small AC current was passed through the torque motor to reduce fractional error, and a microscope increased the accuracy with which the pointer could be set at the fiducial line. These are shown in Figure (19).

The electrobalance was mounted on a special bench to reduce the effects of vibrations and jolts. The bench top was solid marble and rested on cork slabs. The cement block legs, resting on cork feet, were further stabilized by steel cross bars.

2. Calibration of Electrobalance

Normally, the electrobalance was calibrated with National Bureau of Standards, class S, calibrated weights of 1, 2, 3, and 5 milligrams. Since for our purposes, the balance was to be used in the region of 100 to 200 micrograms (0.1 to 0.2 milligrams), a check on the linearity of the balance between 0 and 1 milligram

UNCLASSIFIED
ORNL-LR-DWG. 37877

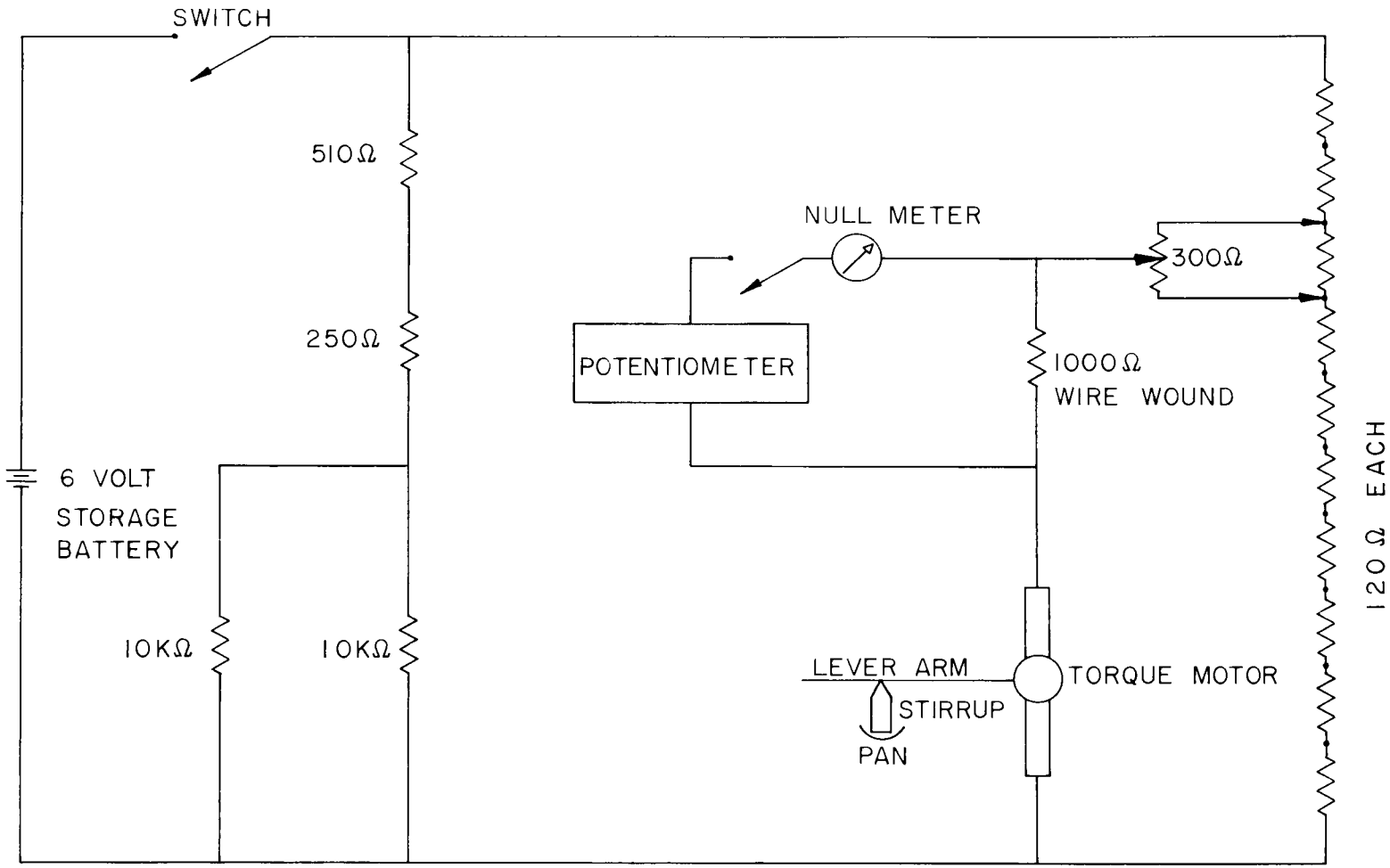

Fig. 18. Modified Circuit for Cahn Electrobalance.

UNCLASSIFIED
PHOTO 45951

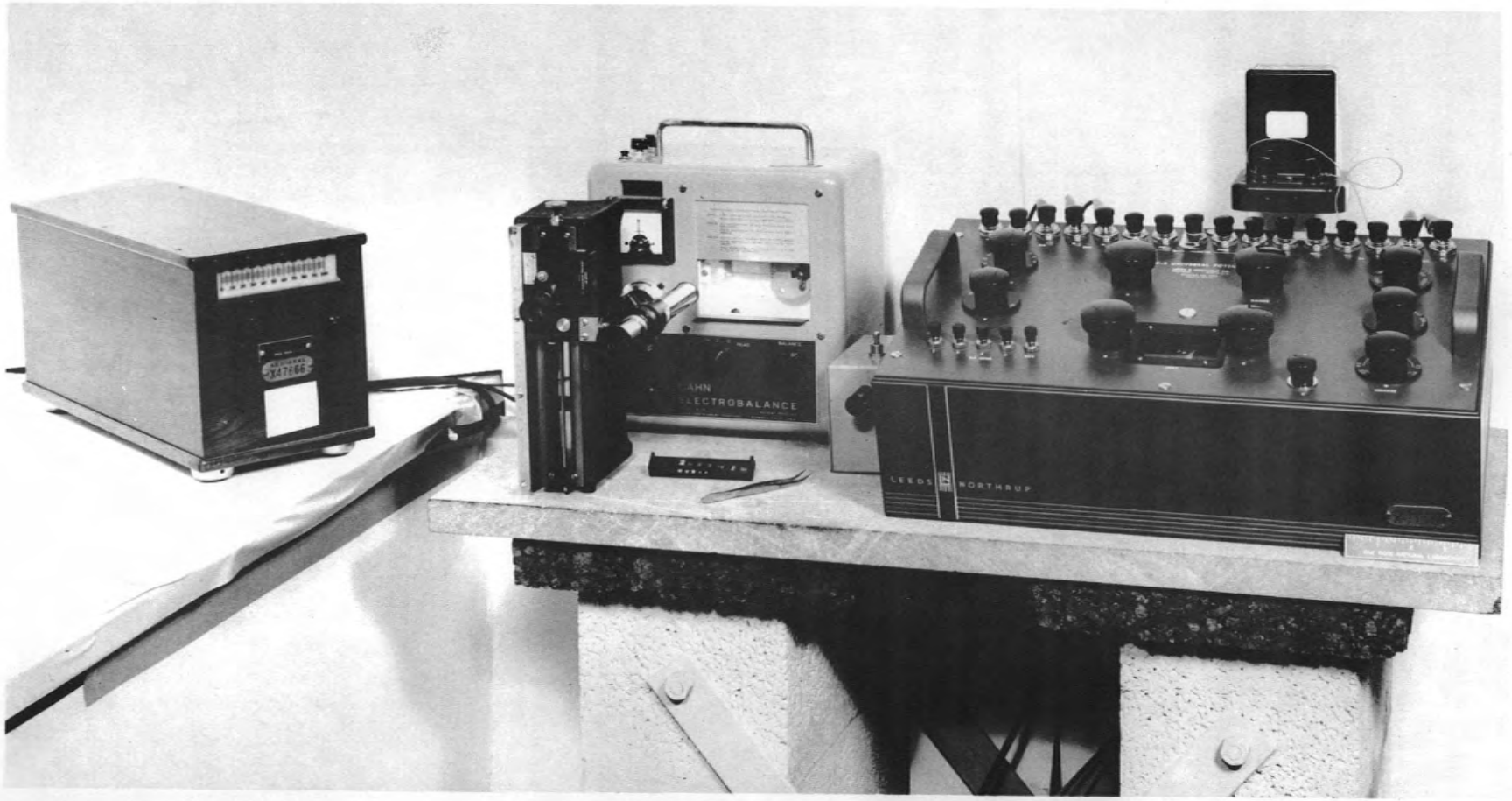

Fig. 19. Cahn Electrobalance with Modifications.

was needed. The following method for calibrating in this range was devised. The balance was first calibrated in the 1 to 5 milligram range using the class S weights. Then a thin wire such as number 40 copper was chosen of sufficient length so that its weight was roughly 1 milligram. After the wire was weighed accurately, it was cut into 10 equal segments. These segments were individually balanced and the corresponding potentials noted. If the original wire was, say, of length ℓ and weight w, and the average length of the segments was $\frac{\ell}{10}$, then the average weight was $\frac{w}{10}$. This average weight corresponded to the average of the ten potentials, thus giving a calibration point in the desired region. (See Table III.)

Figure (20) shows the calibration curve for the electrobalance. The 0.1 milligram and 0.5 milligram points were obtained by the method just described. It may be seen that the curve is linear between 0 and 1 milligram. The calibration curve does not pass through the origin because a small amount of current is necessary to support the empty balance pan and stirrup.

TABLE III

CALIBRATION OF ELECTROBALANCE

A. Initial Calibration

WEIGHT (mg)	0 mg	1 mg	2 mg	3 mg	5 mg
POTENTIAL (v)	0.016338	0.131743	0.244677	0.359590	0.586290

LEAST SQUARES FIT: $W = 8.853V - 0.179$

B. Calibration Point in 0.1 mg Range

Weight of 1 inch of 40 copper wire: 1.15 mg

SEGMENT	POTENTIAL, V_i (volts)
(1)	.031099
(2)	.030930
(3)	.030454
(4)	.031223
(5)	.030996
(6)	.029520
(7)	.030394
(8)	.029868
(9)	.029224
(10)	.029157
ΣV_i	.302865

$\therefore \overline{W}_i = \frac{1.15}{10} = 0.115$ mg corresponds to $\overline{V}_i = \frac{.302865}{10} = .03029$ volts

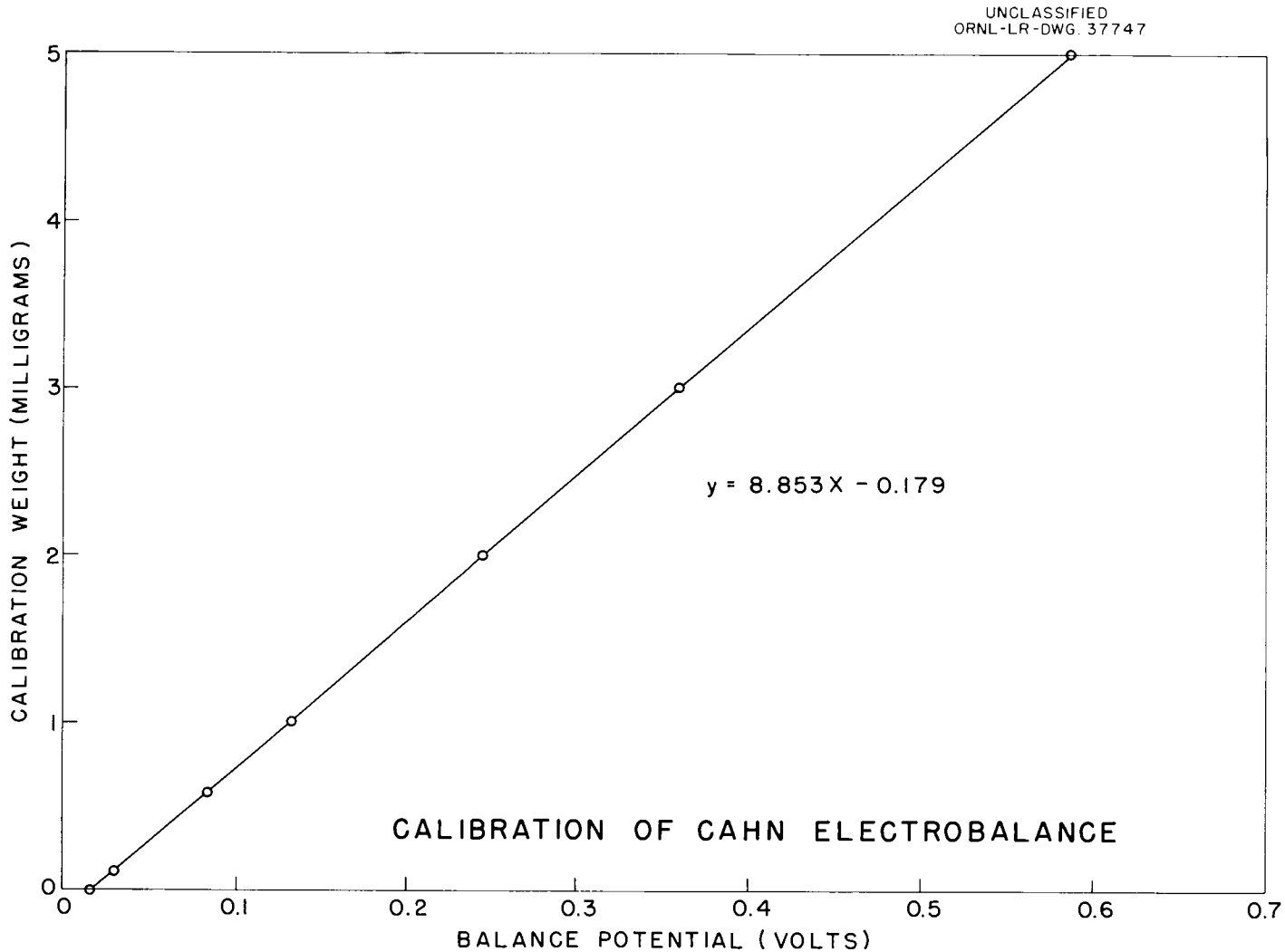

Fig. 20. Calibration of Cahn Electrobalance.

V. PROCEDURE AND RESULTS

To determine the stopping power of a metallic foil, the drift method was used whereby the foil was precooled by Peltier cooling and allowed to warm up under the influence of the beam power.

The apparent energy loss in the foil, $(\overline{\Delta E})_{app}$, was found by determining K_2, C_1, i_B, and $\dot{D}$ experimentally. The path length was then found by weighing a known area of foil to give the foil thickness in micrograms per square centimeter. Finally, the experimental $\overline{\Delta x}$ was obtained by correcting the thickness for the effects of multiple scatter, and the apparent energy losses were corrected for the effects of single scattering. Stopping power was given by $\frac{(\overline{\Delta E})_{exp}}{\overline{\Delta x}}$.

A. Determination of $(\overline{\Delta E})_{exp}$

After mounting a foil in the manner described in Chapter IV, the apparatus was assembled and bolted to the end of the accelerator. The system was evacuated using first the small Duo-Seal pump to lower the pressure to 100 microns of mercury. At this point, the small pump was cut off and the isolation valve was opened allowing the diffusion pump to bring the pressure down to 10^{-6} millimeters of mercury. After pump-down, the system was given a day or two to reach temperature equilibrium with the heater and temperature control on. The deflection of the temperature monitoring galvanometer was then noted.

To determine the energy loss $(\overline{\Delta E})_{exp}$ it was first necessary to evaluate the heat loss constant of the system, K_2, and the calibration constant, C_1.

Referring to equation (13) it is seen that

$$T = T_o + (T_i - T_o)e^{-K_2 t} \tag{54}$$

for $i_B\overline{\Delta E} = 0$.

Then

$$\log_{10}\left(\frac{T - T_o}{T_i - T_o}\right) = -K_2 t \log_{10} e \tag{55}$$

It is quite clear that K_2 may be determined by evaluating the slope of $\log_{10}(T - T_o)$ as a function of time for $i_B\overline{\Delta E} = 0$. That is, from a plot of $\log_{10}(T - T_o)$ vs. t one obtains

$$\text{Slope} = -K_2 \log_{10} e = \frac{\Delta \log_{10}(T-T_o)}{\Delta t} , \tag{56}$$

or

$$K_2 = -\frac{1}{0.435}\left(\frac{\Delta \log_{10}(T-T_o)}{\Delta t}\right) . \tag{57}$$

The foil was precooled by the Peltier effect to some temperature T_i and allowed to drift back toward T_o with $i_B\overline{\Delta E} = 0$. Galvanometer deflection was recorded manually every 0.1 minutes. By plotting the temperature as a function of time on semi-log paper, K_2 was obtained directly from the slope. Figure 21 shows the curve for determining K_2. Temperatures are given in terms of galvanometer deflections. A value of 0.198 min^{-1} was obtained for K_2 in approximate agreement with the theoretically determined value of 0.152 min^{-1}. The discrepancy between the values is to be expected because of the difficulties involved in determining all the heat losses theoretically. The interest

UNCLASSIFIED
ORNL-LR-DWG. 37746

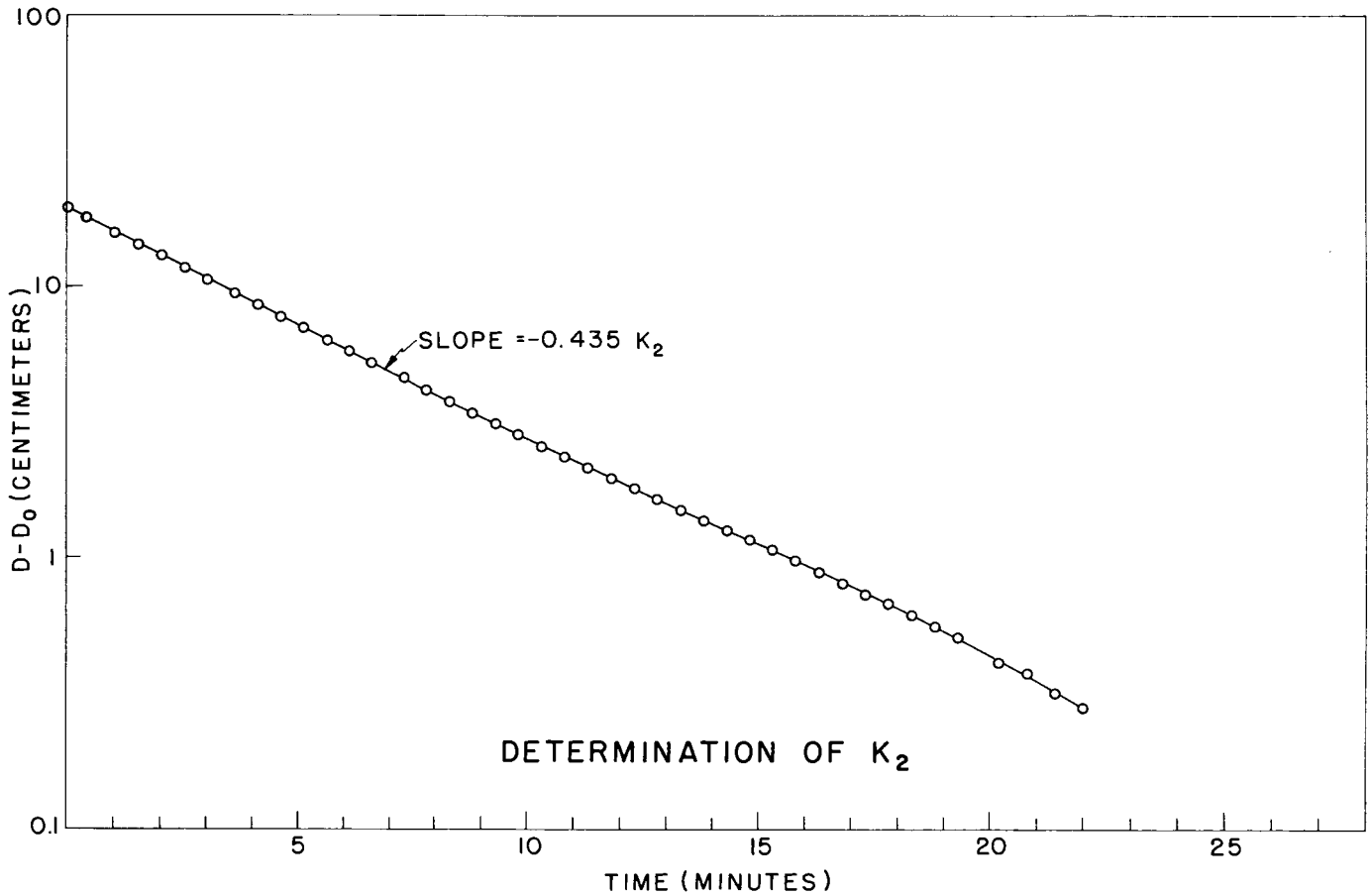

Fig. 21. Determination of K_2.

here was that the system was behaving approximately as calculated from the design.

Note also that all heat losses were attributed to conduction. There was a slight contribution from radiation, but this was thought to be very small compared to the conduction losses.

Using the value

$$K_2 = 0.198^{-1}$$

and assuming a maximum Δt of 0.5 min., the heat loss correction is

$$\frac{\sinh K_2 \Delta t}{K_2 \Delta t} \simeq \frac{\sinh 0.1}{0.1} = \frac{.1002}{.1} = 1.002 \qquad (58)$$

This correction is well within experimental error and may be neglected.

After determining K_2, the power supply for the electron gun was turned on to give an electron beam. The beam energy in this case was due to the second anode potential only. The beam was focused by varying the potential of the electrostatic deflection plates, the current through the degaussing coils, the first anode potential, and the grid potential until a minimum was found in the collimator current as read on the galvanometer G_1. The minimum indicated that most of the beam was not striking the collimator but was passing through the collimating slits and striking the foil. Due to its low energy (of the order of 1 Kev.) the beam was completely stopped by the foil, and the resulting electron current was recorded by the galvanometer G_2. The calibration constant, C_1, could now be determined, for at low beam

energies when the electrons were all stopped the beam dissipated all its energy in the foil. That is, $\overline{\Delta E} = E$, and $i_B = i_F$. The calibration relation was then $i_F E = C_1 \dot{D}$ where i_F is the foil current measured by galvanometer G_2. The foil was first precooled to some temperature T_i below the environmental temperature. The rate of heating due to the beam power absorbed was determined by recording the galvanometer deflection every 0.1 minutes, and the slope of the temperature vs. time curve was taken at $T = T_o$. This gave a value of

$$C_1 \cong 38 \ \frac{\mu \text{ watt}}{\text{cm/min}} .$$

The discrepancy between the theoretical value of C_1 of 29.2 $\frac{\mu \text{ watt}}{\text{cm/min}}$ (see Chapter II) and the experimental value may be attributed in part to the fact that the thermoelectric power of the thermopile was not known accurately. For example, if it were somewhat lower than 240 microvolts per absolute degree, the value of α would be larger, resulting in a greater experimental value of C_1. Again, the theoretical result was simply an indication that the experimental value was of the correct order of magnitude.

This value of C_1 may be further substantiated using the Peltier effect. The Peltier current was previously plotted as a function of $\dot{D}$ in Figure 2. To find C_1 low beam energies were again used so that all electrons were stopped in the foil and $\overline{\Delta E} = E$. The beam heating was then balanced by Peltier cooling. Corresponding to the Peltier current necessary to balance the heating, a value of $\dot{D}$ was read from

the calibration curve (Figure 2). This $\dot{D}$ could be used in the relationship $i_F E = C_1 \dot{D}$ just as in the drift method. The calibration constant, C_1, found by this method was the same as that from the drift method.

After determining the constants K_2 and C_1, the data for stopping power were obtained. The accelerating high voltage was varied from $31._{56}$ to $126._{56}$ Kev in steps of 10 Kev. For a given voltage, the rate of heating due to beam power was recorded by precooling the foil and recording the galvanometer deflections each 0.1 minutes as the deflection passed through the zero point corresponding to T_o. All beam current passing through the foil was collected in the Faraday cup, on the bias discs, or on the foil and foil ring. The apparent energy loss $\overline{\Delta E}_{app}$ was then simply

$$\overline{\Delta E}_{app} = \frac{C_1 \dot{D}}{i_B} \tag{59}$$

B. Determination of $\overline{\Delta x}$

After completing the measurements of $\overline{\Delta E}_{app}$ for various incident energies, it remained to determine $\overline{\Delta x}$, the path length. As indicated previously, the foil thickness was determined by weighing a known area of foil.

The foil and its copper support ring were first removed from their mount using a special "jig" so as to protect the thermocouple wires from unnecessary stress. The foil and ring were then placed on a smooth sheet of formica, and the foil was punched out of the ring using

a razor-sharp circular punch whose diameter was known accurately. This known area of foil was weighed in the electrobalance in the manner described previously.

After finding the foil thickness, it was necessary to correct for multiple scatter effects to find the true path length. Using Williams' theory of multiple scattering, the increase in path length was calculated for each incident energy. These increases were added to the foil thickness to give the path length at each energy.

C. Apparent Stopping Power

The apparent stopping power is given by the ratio of $\frac{\overline{\Delta E}_{app}}{\overline{\Delta x}}$ where $\overline{\Delta E}_{app}$ and $\overline{\Delta x}$ are the quantities just determined. It was pointed out earlier, however, that the apparent stopping power must be corrected for the effects of single scattering. Using Mott's theory of single scattering, the probability for an electron to strike the copper support ring was calculated. If one assumes that all such electrons lose 100% of their energy in striking the ring, the net effect on the stopping power may be calculated. This gave the true experimental stopping power, $\frac{\overline{\Delta E}_{exp}}{\overline{\Delta x}}$.

D. Results

Shown in Figure 22 are the results for the 191.8 microgram per square centimeter copper foil. The stopping power was measured for incident electron energies of $31._{56}$ to $126._{56}$ Kev. The data points have been corrected for single scattering as indicated.

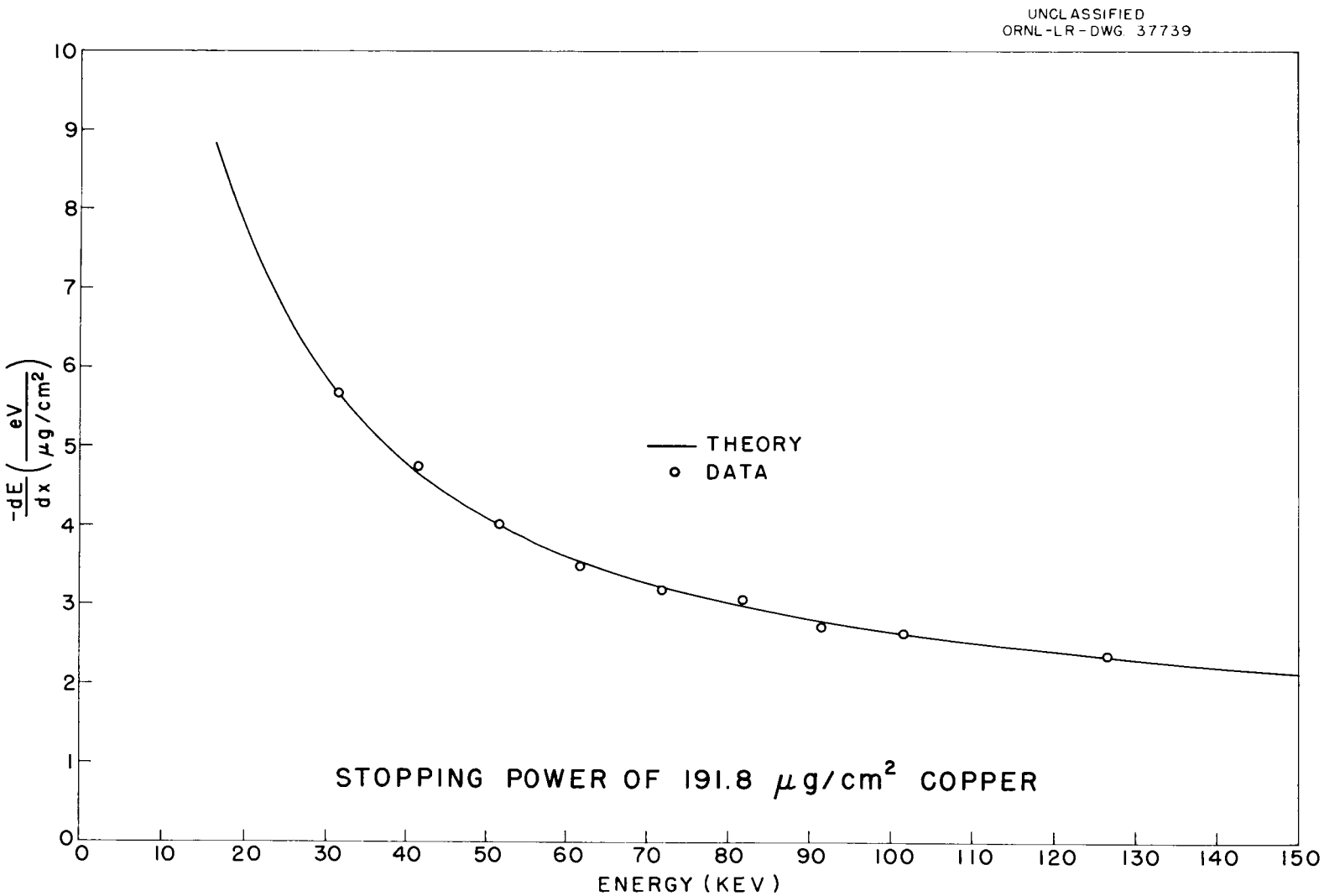

Fig. 22. Stopping Power for 191.8 μg/cm^2 Copper.

VI. CONCLUSIONS

Electron stopping power was studied for a 191.8 $\frac{\mu g}{cm^2}$ copper foil using incident electrons of $31._{56}$ to $126._{56}$ Kev. Energy losses in the foil were measured directly by calorimetric methods. When the experimental results were corrected for single and multiple scattering effects, good agreement was found with Bethe's stopping power theory.

It is felt that these results would be even more reliable if the single scattering correction could be eliminated. Redesign of the system and use of extremely thin foil mounts would eliminate the possibility of single scatter effects.

On the other hand, the results suggest the possibility of using calorimetric techniques of this type for single-scattering studies. The high energy primary electrons scattered from the foil at a particular angle might strike an extra ring with thermocouples. The heating of the extra ring would be a measure of the number of scattered primaries for the angle. Pick-up and recording of extraneous low energy electrons by the detector ring would be minimized because of the small energy they would leave in a calorimetric detector.

APPENDIX I

Temperature Distribution In Thermocouple Wires

Consider a conductor of length ℓ and cross section A connecting two systems whose temperatures are T_o and T_ℓ respectively. One wishes to determine the temperature distribution and heat flow in the conductor when a current i_P passes through the conductor.

If the conductor has a thermal conductivity K and resistance R, then we define

$$K \frac{d^2T}{dx^2} = - \frac{i_P^2 R}{\ell A} \tag{60}$$

or

$$\frac{d^2T}{dx^2} = - \frac{i_P^2 R}{K\ell A} = - C_1 \tag{61}$$

The solutions are

$$\frac{dT}{dx} = - C_1 \; x + C_2 \tag{62}$$

and

$$T = - C_1 \frac{x^2}{2} + C_2 \; x + C_3 \tag{63}$$

The constants of integration may be found from the boundary conditions. At $x = 0$, $T = T_o$; therefore, $C_3 = T_o$; and at $x = \ell$, $T = T_\ell$. Therefore,

$$C_2 = \frac{T_\ell - T_o + \left(\frac{i_P^2 R\ell}{2KA}\right)}{\ell} \tag{64}$$

Substituting in equation (63) and simplifying, we have for the temperature at any point x

$$T = \frac{i_P^2 R}{2K\ell A}\left(\ell x - x^2\right) + \left(T_\ell - T_o\right)\frac{x}{\ell} + T_o \qquad (65)$$

The heat flow is found easily from the relation

$$H = -KA\frac{dT}{dx} \qquad (66)$$

Using the expression for dT/dx from equation (62) and substituting for the values of C_1 and C_2,

$$\frac{dT}{dx} = \left(-\frac{i^2 R}{K\ell A}\right) x + \frac{T_\ell - T_o + \frac{i_P^2 R\ell}{2KA}}{\ell} \qquad (67)$$

Using this value, dT/dx may be substituted into equation (66) to yield

$$H = i_P^2 R\left(\frac{x}{\ell} - \frac{1}{2}\right) - KA\left(\frac{T_\ell - T_o}{\ell}\right) \qquad (68)$$

Referring to the solution for T, one observes that when no electric current flows through the conductor ($i_P = 0$), then the temperature at any point x on the conductor goes linearly with x. However, when a current flows, a quadratic dependence on x is seen.

Another interesting case is when $T_\ell = T_o$ (as in the null method). It is then seen that T has its greatest value at $x = \ell/2$ and is distributed symmetrically about this value. The heat flow is then outward from this point and is the same in both directions. It is for this reason that only 1/2 $i_P^2 R$ is used in computing the Peltier heating, for only 1/2 the Joule heating that arises in the conductor flows into the

system. This fact holds true even when the T_ℓ and T_o are different temperatures, for the heat flow term containing i_P^2R is independent of T_ℓ and T_o so that the Joule heating will always contribute just half to each system. Both of the above cases are shown graphically in Figure (23).

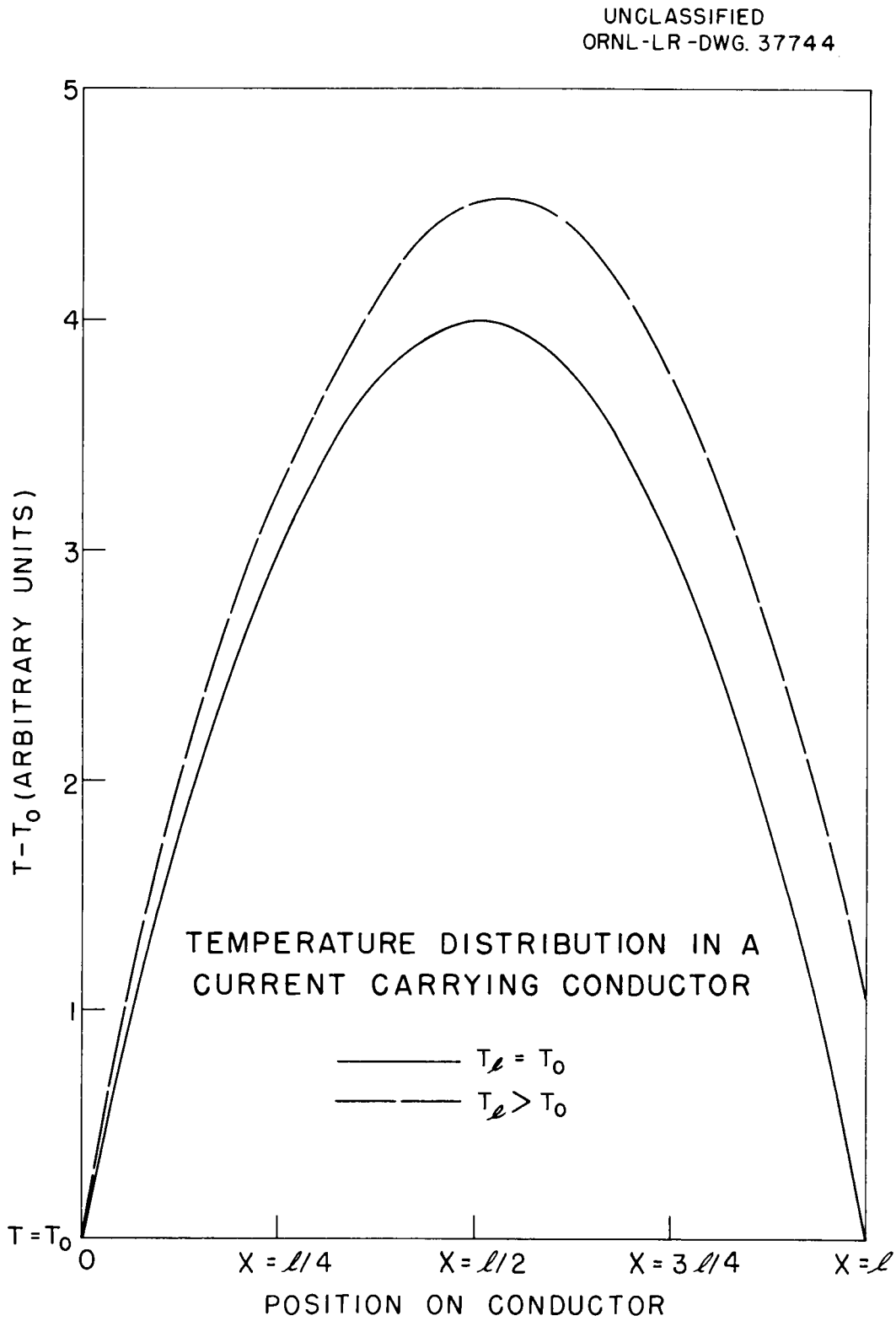

Fig. 23. Temperature Distribution in a Current Carrying Conductor.

APPENDIX E

Temperature Gradient in the Foil

Consider a metallic foil of thermal conductivity k, radius r_2, and thickness x. One is interested in the temperature gradient in the foil when an electron beam with radius of cross section r strikes the foil normally.

If the area of a small shell is $(2\pi r)x$, then the rate of heat transfer across the surface is

$$H = -2\pi r\, x\, k \frac{dT}{dr} \tag{69}$$

where $\frac{dT}{dr}$ is the temperature gradient at the radius r. If the temperature at r_1 is T_1 and at r_2 is T_2, then

$$H \int_{r_1}^{r_2} \frac{dr}{r} = -2\pi\, k\, x \int_{T_1}^{T_2} dT \tag{70}$$

and

$$H = \frac{-2\pi\, k\, x \left[T_2 - T_1\right]}{\ln\left(\frac{r_2}{r_1}\right)} \tag{71}$$

Solving for $(T_1 - T_2)$ and using $H = \frac{P}{J}$ where P is beam power delivered to the foil and J the mechanical equivalent of heat, 4.19 Joules/cal, we have

$$(T_1 - T_2) = \frac{(P/J)\ln\left(r_2/r_1\right)}{2\pi\, k\, x} \tag{72}$$

If $\rho x = 191.8 \frac{\mu g}{cm^2}$ for a copper foil of density $\rho = 8.9 \frac{g}{cm^3}$, $k = 0.918 \frac{cal}{cm\ sec\ C^\circ}$, $r_1 = 3/32$ inch, and $r_2 = 1/4$ inch; then for a typical input power of 250 μwatt, the temperature difference between the "hot spot" where the beam strikes and the outer edge of the foil is $(T_1 - T_2) = 0.474\ C^\circ$.

An estimate of the time required for the heat to travel across the foil may be readily made. It is well known that the time τ for the temperature to change by e^{-1} of its initial value[42] is of the order

$$\tau = \frac{r^2 \rho c}{k} \tag{73}$$

where r is the radial distance from the boundary where the temperature change is impressed, ρ, c, and k are the density, specific heat, and thermal conductivity of the foil material. For copper foil one half inch in diameter $\tau = 0.2$ sec. Thus, any transient heat effects occur in a time small compared to the observation times of about 6 seconds.

[42] See, for instance, H. S. Carslaw and J. C. Jaeger, CONDUCTION OF HEAT IN SOLIDS (Oxford Clarendon Press, 1947), p. 170.

APPENDIX III

Data

Table IV gives a tabulation of the data for the 191.8 microgram per square centimeter copper foil. Incident energies were from 31.56 to 126.56 Kev at intervals of 10 Kev. The calibration constant for these data was 37.6 micro-watts per centimeter per minute with the exception of the 126.56 Kev run. This run was taken on a different day and the calibration constant was 39.9 micro-watts per centimeter per minute.

TABLE IV

Data for 191.8 $\mu g/cm^2$ Copper

E_{Beam} ‡ (Kev)	$\mathring{D}$ (cm/min)	$P=C_1\mathring{D}$* (μwatt)	i_{Beam} † (μamp)	$(\overline{\Delta E})_{app}=\frac{P}{i_B}$ (ev)	f	fE_{Beam} (ev)	$(\overline{\Delta E})_{exp}$ (ev)	$\Delta\ell$ ($\mu g/cm^2$)	$\overline{\Delta x}=t+\Delta\ell$ ($\mu g/cm^2$)	$\left(\frac{\Delta E}{\Delta x}\right)_{exp}$ $\left(\frac{ev}{\mu g/cm^2}\right)$	$\left(\frac{dE}{dx}\right)_{Theory}$ $\left(\frac{ev}{\mu g/cm^2}\right)$
31.56	10.50	395	.2152	1834	.0198	624.89	1234	14.8	206.6	5.97	5.84
41.56	9.76	367	.2639	1391	.0106	446.26	954	8.0	199.8	4.78	4.78
51.56	7.95	299	.2640	1132	.0068	350.61	787	4.9	196.7	4.00	4.10
61.56	6.95	261	.2700	968	.0047	289.33	682	3.2	195.0	3.50	3.63
71.56	4.83	182	.2111	860	.0035	250.46	612	2.3	194.1	3.15	3.28
81.56	4.58	172	.2111	815	.0027	220.21	597	1.8	193.6	3.08	3.02
91.56	4.39	165	.2152	767	.0021	192.28	576	1.3	193.1	2.98	2.80
101.56	4.16	156	.2253	694	.0017	172.65	522	1.0	192.8	2.71	2.63
126.56	3.88	155**	.2740	565	.0011	139.22	426	0.7	192.5	2.21	2.29

* $C_1 = 37.6 \frac{\mu watt}{cm/min}$

** Data for 126.56 KV run taken with $C_1 = 39.9 \frac{\mu watt}{cm/min}$

† $i_{Beam} = i_{Cup}$ since i_{Foil} and i_{Bias} were both negligible compared to i_{Cup}

‡ E_{Beam} = accelerator H.V. plus second anode potential of 1.56 KV.

APPENDIX IV

Sample Calculation

The following is a sample calculation for the stopping power of the 191.8 $\mu g/cm^2$ copper foil. The calibration constant will first be evaluated after which the apparant energy loss $(\overline{\Delta E})_{app}$ for a typical run will be determined. Using single scattering theory, $(\overline{\Delta E})_{exp}$ will be calculated from $(\overline{\Delta E})_{app}$. Finally, the foil thickness, $\overline{\Delta x}$, will be calculated and path length corrections made. The stopping power will then be the ratio of $(\overline{\Delta E})_{exp}/\overline{\Delta x}$.

1. Calibration

Table V gives the data for a typical calibration run. It has previously been shown that the slope, $\mathring{T}$, evaluated when $T \cong T_o$ was just

$$\mathring{T} = \left(\frac{T_+ - T_-}{t_+ - t_-}\right) = K_1 \frac{\ell_B \overline{\Delta E} \sinh K_2 \Delta t}{K_2 \Delta t} \tag{18}$$

or in terms of galvanometer deflection

$$\frac{D_+ - D_-}{t_+ - t_-} = \frac{\ell_B \Delta_E}{C_1} \frac{\sinh K_2 \Delta t}{K_2 \Delta t} \tag{74}$$

If, for example, Δt is chosen to be 0.5 min then $\mathring{D}$ is found by choosing values of $\mathring{D}$ at time $\Delta t = +0.5$ min and $\Delta t = -0.5$ min. Since $K_2 = -0.198$ min^{-1}, then $K_2 \Delta t = 0.99$ and $\sinh K_2 \Delta t / K_2 \Delta t = 1.002$. For the data given

TABLE V

Calibration Run for Copper

Panel Settings		$t-t_o$	D(cm)	$D_1^+-D_1^-$ ($\Delta t=0.1$)	$D_2^+-D_2^-$ ($\Delta t=0.2$)	$D_3^+-D_3^-$ ($\Delta t=0.3$)	$D_4^+-D_4^-$ ($\Delta t=0.4$)	$D_5^+-D_5^-$ ($\Delta t=0.5$)
E_{Beam}	1560 v	-0.5	30.08					
1st Anode	425 v	-0.4	29.17					
E_{Bias}	-750 v	-0.3	28.12					
ℓ_{Foil}	60 mm	-0.2	27.10					
ℓ_{Cup}	4 mm	-0.1	26.08					
ℓ_{Bias}	0 mm	0	25.07	1.98	3.90	5.90	7.67	9.37
ℓ_{Coil}	225 mm	0.1	24.10					
Filament	4.6 amp	0.2	23.20					
Grid	0 v	0.3	22.32					
Cathode	0 amp	0.4	21.50					
Gun Emm.	8.5 μ watt	0.5	20.71					
Pressure	1.6×10^{-5} mm Hg	$D = \frac{D^+-D^-}{2\Delta t}$ $\left(\frac{cm}{min}\right)$		9.90	9.75	9.83	9.59	9.37
T_o	26 cm	$\frac{\sinh K_2\Delta t}{K_2\Delta t}$		1.000	1.000	1.000	1.001	1.002
$T_{precool}$	33 cm							
Time Inter.	0.1 min	$C_1 \left(\frac{\mu\ watt}{cm/min}\right)$		36.78	37.34	37.04	38.00	38.94

$$\mathring{D} = \frac{30.08 - 20.77}{0.5 - (-0.5)} = \frac{9.37 \text{ cm}}{1 \text{ min}} = 9.37 \text{ cm/min} \tag{75}$$

Now

$$i_{Foil} = 60 \text{ mm} \times .00389 \ \mu a/mm = 0.2334 \ \mu a \tag{76}$$

so that

$$i_B \overline{\Delta E} = i_{Foil} E = 0.2334 \ \mu a \times 1560 \text{ v} = 364.1 \ \mu \text{ watt} \tag{77}$$

Then

$$C_1 = \frac{364.1 \ \mu \text{ watt}}{9.37 \text{ cm/min}} \times 1.002 = 38.94 \ \frac{\mu \text{ watt}}{\text{cm/min}} \tag{78}$$

Values of C_1 were obtained in this manner for all intervals of Δt from 0.1 min to 0.5 min. The average of these values was taken to be the calibration constant. Its value was

$$\overline{C_1} = 37.6 \ \frac{\mu \text{ watt}}{\text{cm/min}} \tag{79}$$

2. Determination of $(\ E)_{exp}$

To determine the energy loss $(\overline{\Delta E})_{exp}$ in the foil, values of $\mathring{D}$ were again computed as in the calibration run. The heat loss correction,

$\frac{\sinh K_2\Delta t}{K_2\Delta t}$, was made although it was extremely small. Using the calibration constant previously calculated, the apparent power loss in the foil was $C_1\dot{D}$.

For example, for the 51.56 Kev run (see Table VI), the average $\dot{D}$ was $7.95 \frac{\mu \text{ watt}}{\text{cm/min}}$. The apparent power loss was then $C_1\dot{D} = 299\ \mu$ watt. The total beam current was

$$i_{Beam} = i_{Cup} + i_{Foil} + i_{Bias} = (60+0+0)\text{ mm} \times .00406 \frac{\mu a}{\text{mm}} \tag{80}$$

$$= 0.264\ \mu \text{ amp}$$

Therefore

$$(\overline{\Delta E})_{app} = \frac{P}{i_{Beam}} = \frac{298.92\ \mu \text{ watt}}{0.264\ \mu a} = 1.13 \times 10^3 \text{ ev} \tag{81}$$

The fraction of the beam, f, striking the ring was next computed from single scattering theory. Using Equation (40)

$$f = (\sigma/\sigma_R)\frac{N_A\rho}{A}\, t\, \frac{\pi Z^2 e^4 (1-\beta^2)}{m_o^2 v^4}\left[\frac{1}{\sin^2(\theta_1/2)} - \frac{1}{\sin^2(\theta_2/2)}\right] \tag{40}$$

with $\sigma/\sigma_R = 1.05$; $N_A\rho/A = 8.5 \times 10^{22}$ atoms/cm^3; $t = 191.8\ \mu g/cm^2$; $Z = 29$; $\beta = 0.413$; $v = c\beta$; $\theta_1 = 90°$; $\theta_2 = 112°$; gives $f = 0.0068$ for the 51.56 Kev run.

The value of $(\overline{\Delta E})_{exp}$ could then be found using the relation

$$(\Delta E)_{exp} = \frac{(\overline{\Delta E})_{app} - fE}{1 - f} \tag{47}$$

and gave directly

$$(\overline{\Delta E})_{exp} = 787 \text{ ev} . \tag{82}$$

TABLE VI

Data for 51.56 Kev Run

Settings	
E_{Beam}	51.56 KV
i_{Foil}	0
i_{Cup}	65 mm
i_{Bias}	0
i_{Coll}	0.5 mm
1st Anode	445 v
E_{Bias}	-1000 v
Filament	4.4 amp
Grid	7 v
Cathode	0 amp
Gun Emiss.	6 μa
E-W Coils	3.3 amp
U-D Coils	3.1 amp
I-O Coils	3.35 amp
Defl. Plates	0 volts
Pressure	1.1×10^{-5} mm Hg
T_o	21.1 cm
T (Precool)	30 cm
Time Interval	0.1 min

$t-t_o$	D(cm)	$D_1^+-D_1^-$ (Δt=0.1)	$D_2^+-D_2^-$ (Δt=0.2)	$D_3^+-D_3^-$ (Δt=0.3)	$D_4^+-D_4^-$ (Δt=0.4)	$D_5^+-D_5^-$ (Δt=0.5)
	27.30					
	26.43					
-.5	25.54					
-.4	24.62					
-.3	23.73					
-.2	22.88					
-.1	22.04					
0	21.20	1.63	3.17	4.73	6.32	7.93
.1	20.41					
.2	19.17					
.3	19.00					
.4	18.30					
.5	17.61					
	16.99					
	16.33					
$\dot{D}_{app} = \frac{D^+-D^-}{2\Delta t}$		8.15	7.92	7.88	7.90	7.93
$\frac{\sinh K_2\Delta t}{K_2\Delta t}$		1.000	1.000	1.000	1.001	1.002
$(\dot{D})_{exp}$		8.15	7.92	7.88	7.89	7.91

3. Determination of $\overline{\Delta x}$

The value of $\overline{\Delta x}$, the average path length, was the sum of the foil thickness, t, and the path length increase ℓ due to scattering. To determine the thickness, a known area (0.987 cm^2) of the foil was punched out and weighed on the Cahn electrobalance. The least squares calibration curve used for the copper foil was

$$W = 8.77456\ V - 0.32939 \tag{83}$$

where W is the weight in milligrans and V is the corresponding potential drop. The average balance potential for ten weighings of the foil was $\overline{V}_i = 0.059114$ volts. Using this value in Equation (83) gave the foil weight to be 189.31 μg. The foil thickness, in micrograms per square centimeter was then $\frac{189.31\ \mu g}{0.987\ cm^2} = 191.8\ \frac{\mu g}{cm^2}$.

Path length corrections were calculated from the relation

$$\overline{\Delta \ell} = 1/2 \int_0^t \overline{\theta^2}\ dt \tag{50}$$

where $\overline{\theta^2}$ is the mean square scattering angle given by Equation (51). Using the values Z = 29, $N = 8.5 \times 10^{22}$ atoms/cm^3, $m_o = 9.11 \times 10^{-28}$ gm, and $e^4 = 5.3084 \times 10^{-38}$ erg^2cm^2 and $\beta = v/c$, Equation (51) may be written

$$\overline{\theta^2} = at \log bt \tag{51}$$

where $a = \left[73.0632\ (1 - \beta^2)/\beta^4\right]\ cm^{-1}$

$$b = \left[1.4611 \times 10^5/\beta^2 \right] \text{ cm}^{-1}$$

A substitution of the value of $\overline{\theta^2}$ from Equation (51) into Equation (50) and an integration gives

$$\overline{\Delta \ell} = \frac{at^2}{4} \left(\log bt - \frac{1}{2}\right) \tag{84}$$

Table VII shows the path length corrections made using this relation.

The 51.56 Kev run, for example, had a $\overline{\Delta \ell}$ of 4.9 $\mu g/cm^2$ so that

$$\overline{\Delta x} = 191.8 + 4.9 = 196.7 \ \mu g/cm^2 \tag{85}$$

The final calculation was that of the stopping power itself. This was the ratio of $\frac{(\overline{\Delta E})_{exp}}{\overline{\Delta x}}$. Thus for the 51.56 Kev run

$$\frac{(\overline{\Delta E})_{exp}}{\overline{\Delta x}} = \frac{787.01 \text{ ev}}{196.7 \ \mu g/cm^2} = 4.00 \ \frac{\text{ev}}{\mu g/cm^2} . \tag{86}$$

This value compares well with the theoretical value of 4.10 $\frac{\text{ev}}{\mu g/cm^2}$ for an energy of 51.56 Kev.

TABLE VII

Path Length Corrections for 191.8 $\mu g/cm^2$ Copper

E	β	a	$b(cm)^{-1}$	bt	$\log bt-\frac{1}{2}$	$\frac{at^2}{4}$	$\overline{\Delta\ell}$ (cm)	$\overline{\Delta\ell}(\mu g/cm^2)$
31.56	0.336	5083.480	12.9412×10^5	27.786	2.825	5.85876×10^{-7}	1.6551×10^{-6}	14.8
41.56	0.380	2998.219	10.1182×10^5	21.725	2.578	3.45548×10^{-7}	0.8908×10^{-6}	8.0
51.56	0.418	1975.723	8.3633×10^5	17.957	2.387	2.27704×10^{-7}	0.5435×10^{-6}	4.9
61.56	0.451	1406.865	7.1832×10^5	15.423	2.235	1.62143×10^{-7}	0.3624×10^{-6}	3.2
71.56	0.480	1059.334	6.3414×10^5	13.616	2.111	1.22089×10^{-7}	0.2577×10^{-6}	2.3
81.56	0.503	852.651	5.7750×10^5	12.400	2.018	0.98269×10^{-7}	0.1983×10^{-6}	1.8
91.56	0.530	665.903	5.2014×10^5	11.168	1.916	0.76746×10^{-7}	0.1470×10^{-6}	1.3
101.56	0.551	552.037	4.8125×10^5	10.333	1.833	0.63623×10^{-7}	0.1166×10^{-6}	1.0
126.56	0.595	376.626	4.1273×10^5	8.862	1.682	0.43407×10^{-7}	0.0730×10^{-6}	0.7

$$\overline{\Delta\ell} = \frac{at^2}{4}\left[\ln bt-\frac{1}{2}\right] \quad \text{WHERE} \begin{cases} a = 73.0632\ (1-\beta^2)/\beta^4\ cm^{-1} \\ b = 1.461065\times10^5/\beta^2\ cm^{-1} \\ t = 191.8\ \mu g/cm^2 = 2.1471\times10^{-5} cm \end{cases}$$

APPENDIX V

Error Analysis

Possible sources of experimental error were in the measurement of the beam current, the beam potential (including second anode potential), the foil thickness and path length, and the rate of temperature change of the foil.

1. Beam Current

The foil current galvanometer could be read accurately to 0.2 mm or 0.2% of full scale. Its calibration constant of 3.89×10^{-3} $\frac{\mu a}{mm}$ was correct to 10^{-5} $\frac{\mu a}{mm}$ or 1 part 389. Thus the error in the foil current for a typical reading at half scale or 50 mm was 0.4% in the reading and 0.26% in the calibration. Total probable error was $\Delta i_{Foil} = \sqrt{(.4)^2 + (.26)^2} = 0.5\%$ and the absolute error was .001 μa.

The cup current galvanometer could also be read to 0.2 mm or 0.4% of half scale and was calibrated to 1 part in 406 or .25%. In addition, the instability of the cup current during a run must be considered. This was about equal to 1 mm at half scale (50 mm) or 2%. Probable cup current error was therefore

$$\Delta i_{cup} = \sqrt{(.4)^2 + (.25)^2 + (2)^2} = 2.1\%$$

and the absolute error was .004 μa.

The bias disc current was calibrated to 0.24% and could be read to 0.2 mm or 0.2% of full scale. Maximum probable error at full scale was then

$$\Delta i_{bias} = \sqrt{(.2)^2 + (.24)^2} = 0.3\%$$

and the absolute error (at full scale) of .0001 μa.

The absolute error in the total current was then the square root of the sum of the squares of the absolute error $\Delta i_{Beam} = \sqrt{(.00.)^2 + (.004)^2 + (.0001)^2}$ = .0041 or ~ 2% of beam current.

2. Beam Potential

The second anode potential was read on a 1% electrostatic voltmeter and could be read to within 5 volts or 0.3% for the range used (1500v). Thus the probable error in the second anode potential was ΔE = 1.1%.

The panel meter for reading beam potential was calibrated accurately and was limited mainly by the accuracy with which it could be read, 0.5 Kev. Hence the probable error in the beam potential was as high as 1.7% at 30 Kev and as low as 0.4% at 125 Kev.

3. Foil Thickness

The accuracy of the foil thickness determination was limited by the value of the foil area and by the weight of the foil. The area punched out was known to about 0.2% since the diameter of the punch's edge was accurately measured to be .442 ± .001 inches. Thus, the main source of error in foil thickness was in weighing the foil. It was previously shown in the discussion of the modifications on the electrobalance that the error in weighing was reduced to 0.3%. Probable error in foil thickness was thus $\Delta(\overline{\Delta x}) = \sqrt{(0.2)^2 + (0.3)^2} \cong 0.36\%$.

4. Rate of Temperature Change

The error in rate of temperature change in terms of galvanometer deflection depended on the stability of the zero point on the galvanometer, the accuracy with which the meter scale could be read, and the effect of heat losses in the system.

During a given run, the drift in zero point was at most 0.5 cm so that the maximum error in the subsequent evaluation of drift rate was estimated as 2%. Because heat losses were small when $\dot{D}$ was evaluated about D_o, it was felt that errors in this source were insignificant compared to the other sources of error in drift rate. The meter could be read accurately to 0.02 cm or 0.2% for a typical 10 cm drift. The total probable error in $\dot{D}$ was thus ~ 2.0%.

To estimate the total probable error in the evaluation of stopping power, let us examine the formula used:

$$\frac{dE}{dx} = \left\{ \frac{\text{Power Delivered to Foil}}{i_{Beam}\,\overline{\Delta x}} \right\}$$

$$= \frac{C_1 \dot{D}}{i_{Beam}\,\Delta x} = \frac{\left[\frac{(\text{2nd Anode})(i\ \text{Foil})}{\dot{D}_{Cal}} \right] \dot{D}_{Run}}{(i_{Beam})\,\overline{\Delta x}} \tag{89}$$

The error in beam potential does not enter into the calculation of stopping power but only contributes to the uncertainty in the energy at which the stopping power determination was made. Thus the probable error in the stopping power is

$$\Delta\left(\frac{dE}{dx}\right) = \sqrt{(\Delta E)^2 + (\Delta i_{Foil})^2 + (\Delta\dot{D}_{Cal})^2 + (\Delta\dot{D}_{Run})^2 + (\Delta i_{Beam})^2 + (\Delta\langle\Delta x\rangle)^2}$$

$$= \sqrt{(1.1)^2 + (0.5)^2 + (2.0)^2 + (2.0)^2 + (2.1)^2 + (0.36)^2}$$

$$= 3.7\% \,. \tag{90}$$

Bibliography

Birkhoff, R. D., "The Passage of Fast Electrons Through Matter", Handbuch der Physik, 34, 53 (1958).

Carslaw, H. S., and Jaeger, J. C., CONDUCTION OF HEAT IN SOLIDS (Oxford-Clarendon Press, 1947) p. 170.

Curie, P., and Laborde, A., "Sur La Chaleur Dégagée Spontanément Par Les Sels De Radium", Comp. Rend. 136, 673 (1903).

Doggett, J. A., and Spencer, L. V., "Elastic Scattering of Electrons and Positrons by Point Nuclei", Phys. Rev. 103, 1597 (1956).

Ellis, C. D., and Wooster, B. A., "The Average Energy of Disintegration of Radium E", Proc. Roy. Soc. A-117, 109 (1928).

Gurney, R. W., "Number of Particles in the Beta-Ray Spectra of Radium-B and Radium-C", Proc. Roy. Soc. A-109, 540 (1925).

Holland, L., VACUUM DEPOSITION OF THIN FILMS (Chapman and Hall, Ltd., London, 1956).

Johns, H. E., Bernier, J. P., and Cormack, D. V., "A Direct Measurement of the Energy Locally Absorbed From a Gamma-Ray Beam", Nature 176, 560 (1955).

Kalil, Ford, Stone, W. G., Hubbell, H. H. Jr., and Birkhoff, R. D., "Stopping Power of Thin Aluminum Foils for 12 to 127 Kev Electrons", ORNL-2731, unpublished.

Laughlin, J. S., and Beattie, J. W., "Calorimetric Evaluation of the Roentgen for 400 KV and 22.5 Mev Roentgen Rays", Am. J. Roent. 70, 294 (1953).

Meitner, L., and Orthmann, W., "Über Eine Absolute Bestimmung Der Energie Der Primären B-Strahlen Von Radium E", Zeit. für Physik 60, 143 (1930).

Meyers, O. E., Nucleonics 5, No. 5, 37 (1949).

Moliere, G., "Theorie Der Streuung Schneller Geladener Teilchen. II Mehrfach- und Vielfachstreuung", Z. Naturforsch, 3a, 78 (1948).

Mott, M. F., "The Polarisation of Electrons by Double Scattering", Proc. Roy. Soc., London 135-A, 429 (1932).

Mott, M. F., "The Scattering of Fast Electrons by Atomic Nuclei", Proc. Roy. Soc. London 124-A, 425 (1929).

Neary, G. J., "The B-Ray Spectrum of Radium E", Proc. Roy. Soc. London A-175, 71 (1940).

Rutherford, E., "Scattering of Alpha and Beta Particles by Matter and the Structure of the Atom", Phil. Mag. 21, 669 (1911).

Rutherford, E., and Barnes, H., "Heating Effect of the Radium Emanation", Phil. Mag. 7, 202 (1904).

Rutherford, E., and Henderson, M.C., "The Heating Effects of Radium and Its Emanation", Phil. Mag. 25, 312 (1913).

Seitz, F., and J. S. Koehler, SOLID STATE PHYSICS, (Academic Press, New York, Volume 2, 1956) p. 309.

Watson, S. W., and Henderson, M. C., "The Heating Effects of Thorium and Radium Products", Proc. Roy. Soc. A-118, 318 (1928).

Williams, E. J., "Concerning the Scattering of Fast Electrons and of Cosmic-Ray Particles", Proc. Roy. Soc. 169-A, 531 (1939).

Williams, E. J., "Multiple Scattering of Fast Electrons and Alpha-Particles and 'Curvature' of Cloud Tracks Due to Scattering", Phys. Rev. 58, 292 (1940).

ORNL-2775
Physics and Mathematics
TID-4500 (15th ed.)

INTERNAL DISTRIBUTION

1. C. E. Center
2. Biology Library
3. Health Physics Library
4-5. Central Research Library
6. Reactor Experimental Engineering Library
7-26. Laboratory Records Department
27. Laboratory Records, ORNL R.C.
28. L. B. Emlet (K-25)
29. J. P. Murray (Y-12)
30. A. M. Weinberg
31. J. A. Swartout
32. E. D. Shipley
33. M. L. Nelson
34. K. Z. Morgan
35. S. C. Lind
36. A. S. Householder
37. C. S. Harrill
38. C. E. Winters
39. A. H. Snell
40. E. H. Taylor
41. W. H. Jordan
42. T. A. Lincoln
43. A. Hollaender
44. F. L. Culler
45. H. E. Seagren
46. D. Phillips
47. M. T. Kelley
48. E. E. Anderson
49. R. S. Livingston
50. C. P. Keim
51. K. E. Cowser
52. C. D. Susano
53. L. B. Farabee
54. F. J. Davis
55. R. J. Morton
56. C. E. Haynes
57. E. G. Struxness
58. W. E. Cohn
59-109. H. H. Hubbell, Jr.
110. D. E. Arthur
111. J. Neufeld
112. M. J. Skinner
113. J. C. Hart
114. T. H. J. Burnett
115. W. J. Lacy
116. G. S. Hurst
117. T. E. Bortner
118. J. A. Lane
119. P. M. Reyling
120. L. B. Holland
121. J. L. Gabbard
122. R. A. Charpie
123. D. M. Davis
124. P. E. Brown
125. E. D. Gupton
126. J. C. Ledbetter
127. R. L. Clark
128. G. C. Cain
129. L. C. Johnson
130. W. W. Ogg
131. O. D. Teague
132. E. L. Sharp
133. E. J. Kuna
134. H. H. Abee
135. C. R. Guinn
136. A. D. Warden
137. C. C. Sartain
138. J. R. Muir
139. J. A. Auxier
140. M. F. Fair
141. S. I. Auerbach
142. G. W. Royster, Jr.
143. R. R. Dickison
144. F. W. Sanders
145. F. C. Maienschein
146. W. J. Boegly, Jr.
147. F. L. Parker
148. W. E. Lotz
149. B. Fish
150. M. B. Edwards
151. F. M. Empson
152. G. G. Robeck
153-202. R. D. Birkhoff
203. R. H. Ritchie
204. J. A. Harter
205-214. R. M. Johnson
215. J. S. Cheka
216. P. N. Hensley
217. R. W. Peelle
218. D. R. Nelson
219. E. B. Wagner
220. W. Kofink
221. C. A. Preskitt

222. J. C. Frye (consultant)
223. W. H. Langham (consultant)
224. R. L. Platzman (consultant)
225. L. S. Taylor (consultant)
226. A. Wolman (consultant)
227. R. E. Zirkle (consultant)
228. ORNL - Y-12 Technical Library, Document Reference Section

EXTERNAL DISTRIBUTION

229. Knolls Atomic Power Laboratory, Schenectady (R. J. Feinberg)
230. Capt. J. C. Villforth, 58 Diana Lane, West, Fairbarn, Ohio
231. W. O. Olson, 328 Liberty Street, Mankato, Minn.
232. A. P. Hull, Industrial Reactor Laboratories, Inc., Plainsboro, N.J.
233. W. G. Stone, Redstone Arsenal, Huntsville, Ala.
234. F. Kalil, 314 Grovethorn Road, Baltimore 20, Maryland
235. J. S. Laughlin, Dept. of Physics, Memorial Center, Sloan-Kettering, New York 21, N.Y.
236. S. Berk, 1334, Frankford Arsenal, Philadelphia 37, Pa.
237. W. B. Mann, National Bureau of Standards, Chief, Radioactivity Section, Washington 25, D.C.
238. W. C. Roesch, 2413 Tinkle Street, Richland, Wash.
239. G. D. Adams, Jr., Radiological Laboratory, University of California Medical Center, San Francisco 22, Calif.
240-254. P. L. Zeimer, 305 N. Salisburg Ave., Apt. 2-N, West Lafayette, Indiana
255. P. Gaskins, Aloe Scientific Co., Olive Branch, Miss.
256. R. S. Rainey, Box 47-90, Boeing Airplane Co., Seattle 24, Wash.
257. J. Ovadia, Chief Physicist, Michael Reese Hospital, 29th St. and Ellis Ave., Chicago 16, Ill.
258. E. T. Arakawa, Atomic Bomb Casualty Commission, MCAF, Navy 955, c/o FPO, San Francisco, Calif.
259. Division of Research and Development, AEC, ORO
260-869. Given distribution as shown in TID-4500 (15th ed.) under Physics and Mathematics category (75 copies - OTS)
870. L. Scaggs, Argonne Cancer Research Hospital, Chicago 37, Ill.